EFFECT OF AN ALKYL CHAIN ADDITION TO METALLOPORPHYRINS ON BLUE LIGHT PHOTODYNAMIC INACTIVATION OF ESKAPE AND ATYPICAL PATHOGENS

by

Sulaiman Alshehri

A Thesis Submitted in

Partial Fulfillment of the

Requirements for the Degree of

Master of Science

in Biomedical Sciences

at

The University of Wisconsin-Milwaukee

December 2023

ABSTRACT

EFFECT OF AN ALKYL CHAIN ADDITION TO METALLOPORPHYRINS ON BLUE LIGHT PHOTODYNAMIC INACTIVATION OF ESKAPE AND ATYPICAL PATHOGENS

by

Sulaiman Alshehri

The University of Wisconsin-Milwaukee, 2023
Under the Supervision of Professor Troy Skwor

The trending rise in antibiotic resistance poses an enormous public health threat. These antimicrobial-resistant infections not only create an economical burden on individuals and healthcare systems, but also lead to prolonged hospitalizations and mortality rate. Among those highly resistant bacteria are the ESKAPE pathogens, which defines a group of Gram-positive and -negative bacteria that has been associated with multidrug resistant nosocomial infections. They represent more than 40% of species isolated from bloodstream infections exhibiting increased resistance to empirical antimicrobial therapy, length of hospitalization, cost of clinical care, and mortality rate compared to non-ESKAPE pathogens. Therefore, an alternative treatment approach to antimicrobials is warranted. Photodynamic inactivation (PDI) is a potential alternative treatment against these pathogens. It relies on incubating the targeted bacteria with an excitable photosensitizer (PS) chemical agent in the presence of oxygen molecules and the microorganism. Then, utilizing visible light at an appropriate wavelength to transition PS molecules into an excited state creates reactive oxygen species (ROS) that ultimately damage bacterial cells. One of the more commonly studied PS molecules are tetra-cationic TMPyP porphyrin derivatives. Previously, we have shown that among multiple metalloporphyrin derivatives, PdT4 and ZnT4 had the strongest bactericidal effects against methicillin-resistant *Staphylococcus aureus* (MRSA) and *Escherichia coli* using a portable 405 nm LED light. Here

we aimed to determine the impact of adding C14 alkyl chain to PdT4 and ZnT4 on bacterial binding as well as on PDI antimicrobial outcome against an array of ESKAPE pathogens as well as resilient *Bacillus cereus* endospores. Therefore, binding assays were performed to measure the quantity of porphyrins bound to ESKAPE pathogens. We also assessed the PDI bactericidal efficacy using 405 nm LED for the PdT4 and PdC14 as well as 430 nm LED for the ZnT4 and ZnC14 metalloporphyrin derivatives against selected species of the ESKAPE pathogens and *B. cereus* endospores. To determine how much of the bactericidal PDI outcome correlates to both bound versus unbound portions of the PdT4 and PdC14, a binding dependence assay was performed. Our findings show an increased bacterial binding whereby 79% and 68% of total PdC14 was detected in *Enterococcus faecium* and *A. baumannii* respectively, compared to 0% binding associated with PdT4. Relative to ZnT4, ZnC14 shows binding improvement whereby 49% and 80% binding occurred compared to only 2% and 0% ZnT4 detection in both MRSA and *A. baumannii*. Overall, both metalloporphyrin show strong PDI bactericidal activity against both Gram-positive and Gram-negative bacteria. PDI against Gram-positive *E. faecium* resulted in 99.96% reduction using PdC14 at 0.3125 J/cm^2 whereas PdT4 showed lower reduction rate at 97.82%. In Gram-negative *A. baumannii*, 99.88% bacterial reduction rate was achieved using PdC14 at 5 J/cm^2 irradiance whereas PdT4 showed 90.97% . ZnC14 shows >99.99% killing rate of *A. baumannii* whereas ZnT4 only shows 9.74% reduction using 0.25 J/cm^2 irradiance. MRSA also showed 9.00E+07 log inactivation (>99.99%) using ZnC14 at 0.25 J/cm^2 irradiance. Overall, these data highlight metalloporphyrin improvement as a PS in bacterial binding and PDI antimicrobial activity upon insertion of lipophilic C14 alkyl chain.

TABLE OF CONTENTS

LIST OF FIGURES

LIST OF TABLES

LIST OF ABBREVIATIONS

AMR	Antimicrobial resistance
CFU	Colony forming unit
CFU/ml	CFUs per milliliter
LB	Luria broth
TSB	Trypticase soy broth
TSA	Trypticase soy agar
PS	Photosensitizer
PDI	Photodynamic inactivation
A.U.	Absorbance unit
GLASS	Antimicrobial Resistance and Use Surveillance System
MRSA	Methicillin-resistant *Staphylococcus aureus*
WHO	World Health Organization
CDC	Centers for Disease Control and Prevention
TMPyP	5,10,15,20-tetrakis(1-methylpyridinium-4-yl)-porphyrin tetra(p-toluenesulfonate)
MDR	Multidrug resistant
ESKAPE	*Enterococcus faecium*, *Staphylococcus aureus*, *Klebsiella pneumoniae*, *Acinetobacter baumannii*, *Pseudomonas aeruginosa*, and *Enterobacter* species
$^1O_2$	Singlet oxygen
LED	Light emitting diode
J/cm^2	Joule per centimeter square
PdT4	Tetra-cationic palladium TMPyP derivative
ZnT4	Tetra-cationic zinc TMPyP derivative
PdC14	C14 substituted tetra-cationic palladium TMPyP derivative
ZnC14	C14 substituted tetra-cationic zinc TMPyP derivative
ROS	Reactive oxygen species
OD	Optical density
PBS	Phosphate buffer saline
nm	Nanometer
w/v	Wight per volume
RPM	Rotations per minute
SDS	Sodium Dodecyl Sulfate
BSL	Biosafety level

ACKNOWLEDGEMENTS

There are so many people to be grateful for in my life that I wouldn't know how or where to begin. But first, I would like to start with my parents who have given me their unconditional love and relentless support. It has been extremely challenging, for me and for them, to travel across the planet and just be gone for over two years with very little spare time to relax or come back and visit. Yet, they've always asked me to keep my focus on my school/research and make them proud. I hope was able to do that. No words in both languages I speak can ever express my deep gratitude for you.

Dr. Skwor has been instrumental in shaping my research and academic path during the time I was here at UWM. He inherited a struggling student with a lot of obstacles in his way, and then turned him into a scientist. It is hard for me at times to grasp the magnitude of my development over the short time I had spent in his lab. For everything you've done for me, thank you! I really couldn't have asked for a better mentor.

Dr. Nardelli, Dr. Eells, Dr. Doll, and Dr. Liedhegner thank you for being there for me whenever I needed help. Through my journey's ups and downs, you have been my family here at UWM.

I also would like to thank my lab mates and my friends Brandon, Brooke, Alia, and Anthony for their help and support during my time at the lab. And for keeping up with my extremely proficient English. I owe you a lot of gratitude for drawing a smile on my face every time I see you.

CHAPTER 1: BACKGROUND

I. Introduction

1. Antibiotic resistance

Almost one century has passed since the discovery of the first antibiotic agent, penicillin, in 1928 (American Academy of Pediatrics, 2019). Since then, antibiotics have been used worldwide as the treatment of choice for numerous bacterial infections. Eventually, this led to the emergence of many antimicrobial resistant strains of pathogenic bacteria (Tacconelli et al., 2018). One of the major factors in the observed rise of antimicrobial resistance is the global overconsumption of antibiotics among people as well as in agriculture, especially broad-spectrum antibiotics (Van Boeckel et al., 2014). Antimicrobial resistance (AMR) is described as a change in bacteria that occurs overtime where they no longer respond to antibiotics rendering them more difficult to treat clinically (World Health Organization (WHO), 2021). As a result, the Centers for Disease Control and Prevention (CDC) has declared antimicrobial resistance as an urgent public health threat in which 2.8 million infections occur per year in the United States alone (Centers for Disease Control and Prevention (CDC), 2022). In addition, infections due to resistant pathogens have created an economical burden on governments, healthcare system, and patients alike (Thorpe et al., 2018).

The World Health Organization (WHO) launched the Global Antimicrobial Resistance and Use Surveillance System (GLASS) in 2015, which is a global standardized reporting system that functions to collect, analyze, and interpret collected data regarding AMR pathogens with the aim of tracking worldwide AMR trends (World Health Organization (WHO), 2021). Through GLASS, the resistance rate to ciprofloxacin, a commonly prescribed fluoroquinolone antibiotic

to treat urinary tract infections (UTI), has been reported to be at an average of 50% for *Escherichia coli (E. coli)* associated with UTI cases and 42% for *Klebsiella pneumoniae* in countries that are reporting to the WHO GLASS program. In 2019, methicillin-resistant *Staphylococcus aureus* (MRSA) and third-generation cephalosporin resistant *E. coli* blood-stream infections were reported worldwide and evident in 25 and 49 countries, respectively (World Health Organization (WHO), 2021).

Over the years, multiple factors have set the stage for the current rise in AMR occurrence due to increased prevalence of antibiotic resistance genes (ARGs). For example, ARGs have been detected in wastewater all over the world (Mao et al., 2015; Rodriguez-Mozaz et al., 2015; Sabri et al., 2020). Because antibiotics are barely degraded upon administration in both humans and animals, this leads to an increased exposure of bacteria to antibiotics eliminated through urine and feces in wastewater. One study that investigated the relationship between the number of bacterial resistance genes and their corresponding antibiotic concentrations in a wastewater treatment plant in Michigan, revealed that there is a positive correlation between sulfonamides concentrations and *sul1* resistance gene (Gao et al., 2012). This suggests that the presence of unmetabolized antibiotics at subinhibitory concentrations in wastewater facilitates increased resistance levels among bacteria. Consequently, this creates an environment for the bacteria to be continuously exposed to antimicrobial agents and to become resistant over time. Therefore, alternatives to antimicrobial agents are needed.

Another factor that contributes to the increased AMR is the bacteria's ability to exchange ARGs through horizontal gene transfer (Seier-Petersen et al., 2014; Zhang et al., 2017). Resistance genes can be exchanged as a survival mechanism between one bacterium and another, intra-species or inter-species, when coexisting in the same habitat (Zhang et al., 2017).

Furthermore, antibiotics at subinhibitory concentrations have been shown to cause enough stress to stimulate horizontal gene transfer among bacteria (Jutkina et al., 2016). Hence, the need to mitigate the global overconsumption of antibiotics to reduce bacterial exposure to these agents, which may eventually result in selecting resistant strains to overpopulate and become public health threats (Van Boeckel et al., 2014).

2. ESKAPE pathogens

ESKAPE is a term that was coined to distinguish some of the most common multidrug resistant (MDR) bacterial pathogens. This group of pathogens has been shown to be a leading cause of MDR nosocomial infections worldwide, especially in immunocompromised patients (Kondo et al., 2021; Li et al., 2021; Pandey et al., 2021). ESKAPE is an acronym that identifies highly virulent MDR bacteria: *Enterococcus faecium*, *Staphylococcus aureus*, *Klebsiella pneumoniae*, *Acinetobacter baumannii*, *Pseudomonas aeruginosa*, and *Enterobacter* species (Rice, 2008). This group of organisms has been categorized by both the CDC and the WHO as a threat to human public health (Centers for Disease Control and Prevention (CDC), 2019; World Health Organization, 2017). Within this group, Carbapenem-resistant *Acinetobacter* and Carbapenem-resistant *Enterobacteriaceae* are currently classified as urgent threats according to the CDC (Centers for Disease Control and Prevention (CDC), 2019). ESKAPE pathogens have gained resistance against multiple antimicrobial classes including macrolides, tetracyclines, linezolid, fluoroquinolones, β-lactams, β-lactamase inhibitors, and last defense antibiotics such as carbapenems and vancomycin (D. M. P. De Oliveira et al., 2020; Giddins et al., 2018; Herc et al., 2017; Iguchi et al., 2016; Paterson & Bonomo, 2005).

This class of organisms is among the most prevalent bacteria in cutaneous infections (Heitkamp et al., 2018; Masoud et al., 2022). It has been found that ESKAPE pathogens accounted for more than 42% of species isolated from bloodstream infections in the United States alone (Marturano et al., 2019). These infections were associated with a lengthier hospitalization, a $5,500 increased cost of care, and increased mortality rate compared to non-ESKAPE pathogens (Marturano et al., 2019).

3. Wound infections

The skin layer provides a physical protective barrier against bacteria and therefore is considered as a critical component of the innate immune system. Thus, the presence of a wound creates a direct pathway for pathogenic organisms to contaminate the injured physical barrier resulting in abscess-associated inflammation and potential bacteremia if left untreated (Fakhry et al., 2022). Wound infections can originate from small skin lesions, acute traumatic injuries, burn injuries, or surgical interventions. In fact, many nosocomial infections have been linked to wounds induced by surgical interventions and prolonged hospitalization (Hsu et al., 2019). Although *S. aureus* is the most common pathogen associated with skin and soft tissue infections, *P. aeruginosa*, *A. baumannii*, and *Enterococcus faecalis* are also common wound pathogens especially within healthcare facilities (Fakhry et al., 2022; Fleming et al., 2017; Klevens et al., 2007; Prasad et al., 2020). Clinically, cases of skin and soft tissue infections are treated immediately with empirical antibiotic therapy that targets methicillin-resistant *S. aureus* (MRSA); however, it has been estimated that up to 60% of wound infected hospitalized patients have not been responsive to treatment (Amara et al., 2013).

4. Atypical pathogens

Bacillus is a bacterial genus characterized by its ability to transition between two biological states, the vegetative and the endospores, rendering it one of the most resilient life forms. The vegetative form is where this genus is metabolically active and can replicate. The other is the endospore form, which is a highly resilient cell type, allowing *Bacillus* to withstand harsh environments that other non-spore bacteria cannot tolerate. The determinant for which state this genus exists at is the nutrient availability, which is sensed by the bacterium (Rosenberg et al., 2012). This feature gives *Bacillus* the flexibility to undergo either sporulation or germination processes in order to adapt to its environment. For example, multiple species of this genus have been recovered from the Canadian High Arctic, which is characterized as an environment of low nutrients and extremely cold with a mean annual air temperature of -19.7 ˚C (Steven et al., 2007). Due to its resilient nature, *Bacillus* can be thought of as a benchmark to test the range of bactericidal efficiency of PDI against infectious organisms, particularly its endospores.

Although most *Bacillus* species are non-pathogenic in nature and reside mainly in the soil, *Bacillus anthracis* and *Bacillus cereus* are well known human pathogens that have been mostly commonly associated with anthrax and food poisoning, respectively (Kubota et al., 2022; Tan et al., 2014). *Bacillus* is also a major skin and wound pathogen especially prevalent among injection drug users (Sanchez et al., 2021). In addition, *B. anthracis* has been utilized as a biological weapon in bioterrorism (Dull et al., 2002). Moreover, *Bacillus* has been shown to acquire β-lactam resistance further complicating its treatment (Bartoszewicz & Czyżewska, 2021).

Overall, MDR resistant pathogens represent a looming global public health threat. Considering the decrease in discovering new antibiotics in recent times and the increased bacterial resistance against the already existing agents, there is urgency in finding new effective alternative approaches to conventional antibiotics in order to combat the rapidly emerging MDR bacterial strains.

5. Photodynamic inactivation

Photodynamic inactivation (PDI) is the combined use of light and PS to kill pathogenic organisms and is an alternative method to using antimicrobial agents through which various types of pathogenic organisms can be targeted (V.T et al., 2019). PDI has been shown to be effective against both Gram-positive and Gram-negative bacteria (Gamelas et al., 2022; Garcez et al., 2013; Sharma et al., 2020; Skwor et al., 2016), as well as bacteriophages (Heffron et al., 2021). The principle by which PDI works to eradicate microorganisms involves three key elements: a light emitting diode (LED) source, a photoactivable chemical photosensitizer (PS), and oxygen molecules. The light works as an energy source for the PSs to be transitioned from their ground energy state into an excited state. Following the absorption of light, the excited PS chemicals donate electrons to nearby oxygen molecules leading to the formation of reactive oxygen species (ROS), which ultimately can lead to bacterial oxidative stress, cell wall damage, and lysis (Huang et al., 2012).

A PS is in the ground state before photon energy absorption. This ground state PS is characterized by having two electrons with opposing spins at a low energy orbit (Castano et al., 2004). A singlet excited state PS molecule (^{1}PS*) is a photon energized form comprising one excited electron which is boosted into a higher energy orbit (Castano et al., 2004). The energized ^{1}PS* electron can lose its gained energy through either fluorescence, the process of emitting

light, or simply through the internal conversion of absorbed energy into heat. However, this excitation produces short half-life ^{1}PSs* that can lose their gained energy within a timeframe of nanoseconds (Castano et al., 2004). Alternatively, ^{1}PSs* can undergo an intersystem crossing resulting in the formation of a highly energized triplet PS molecule (^{3}PS*) (Castano et al., 2004). Unlike ^{1}PS* molecules, the ^{3}PS* molecule is characterized by having a longer half-life with a timeframe of microseconds and by its ability to transfer its photon absorbed energy to three oxygen molecules ($3O_2$) creating a singlet oxygen ($^{1}O_2$) (Castano et al., 2004). Once the energy is transferred to oxygen, the ^{3}PS* loses its gained energy and reverts to the ground state PS (Castano et al., 2004).

The production of ROSs in PDI follows two main photochemical pathways, type-1 and type-2 (Huang et al., 2012). In type-1 PDI, the photoactivated PS* transfers its electron or proton directly to either the cell membrane itself if nearby or to another substrate. This process forms free radical anions such as superoxide anion, hydrogen peroxide, and hydroxyl radical resulting in damage to the targeted cells (Chandra et al., 2022; Huang et al., 2012). However, type-1 damage is limited and is highly dependent on the ability of the targeted biological cell to produce anti-oxidant enzymes such as superoxide dismutase (SOD), which ultimately reduces the bactericidal effectiveness of PDI (Kimáková et al., 2017; Surur et al., 2022). In type-2 PDI on the other hand, a triplet-state PS (^{3}PS*) transfers its energy directly to an oxygen molecule creating a singlet oxygen ($^{1}O_2^{\cdot}$), a highly oxidizing cytotoxic molecule. The quantity of its production has been used as measurement of PDI efficiency (Ragàs et al., 2010, 2013). Therefore, the production of singlet oxygen molecules through type-2 mechanism is essential for a potent and effective PDI treatment.

PDI efficacy depends on multiple factors, including the type of PS in conjunction with the light source. A commonly used PS is 5,10,15,20-tetrakis(1-methylpyridinium-4-yl)-porphyrin tetra(p-toluenesulfonate) (TMPyP). This porphyrin is characterized by a 420 nm Soret peak, maximum light absorption, with multiple Q-bands at 530 nm and 570 nm wavelengths up to 630 nm (Skwor et al., 2016). Generally, tetra cationic TMPyP derivatives have been shown to be effective in killing both Gram-positive and Gram-negative bacteria (Eichner et al., 2013; Muehler et al., 2022; Schulz et al., 2022; Skwor et al., 2016). Due to the thick negatively charged peptidoglycan cell wall of Gram-positive bacteria, there is an ionic attraction between cationic TMPyP molecules and Gram-positive organisms (Nitzan et al., 1995). However, studies have shown that PDI of Gram-negative bacteria require either a higher concentration of TMPyP derivatives or a longer irradiation time to produce the same bactericidal effect observed with Gram-positive bacteria, possibly due to the presence of a lipopolysaccharides (LPS) outer membrane which is lipophilic in nature (Alves et al., 2009; Muehler et al., 2022). This indicates that the biological structure of the targeted organism may play a major role in the efficiency of PDI.

Another factor to consider in terms of PDI antimicrobial efficiency is the wavelength and irradiance dose of light used to kill organisms. Although the short wavelength of blue light comes with limited tissue penetration, 405 nm blue light is quite effective in killing bacteria in both planktonic suspensions and biofilms (Ferrer-Espada et al., 2019; Lu et al., 2020) as well as *in vivo* (Xuan et al., 2019). Longer wavelength lights (e.g. green and red) have deeper penetration into tissues and the use of light alone has been shown to induce wound healing and promote angiogenesis (Albarracin et al., 2011; de Vasconcelos Catão et al., 2015; do Amparo Manoel et al., 2022).

In a previous publication, PDI with multiple metalloporphyrin derivatives were evaluated for their bactericidal activity against MRSA and *E. coli* (Skwor et al., 2016). The major findings showed that 405 nm blue LED light with the tetra-cationic palladium TMPyP derivative (PdT4), produced the highest bactericidal effect against both MRSA and *E. coli* compared to other metalloporphyrin derivatives (Skwor et al., 2016). In addition, the zinc metalloporphyrin (ZnT4) produced considerable bactericidal activity albeit less than the PdT4 (Skwor et al., 2016). This is most likely due to the red shift of the Soret peak of the ZnT4 being closer to 450 nm wavelength compared to the PdT4 which was at 418 nm. Therefore, the ZnT4 was less excited at the 405 nm blue LED light used in this experiment. Interestingly, MRSA showed a considerable higher susceptibility to PDI with PdT4 compared to *E. coli* (Skwor et al., 2016). This is possibly due to the biological structure composition in Gram-negative bacteria and the presence of a lipophilic outer membrane which repels the hydrophilic positively charged PdT4. As a result, our lab would like to test out a novel metalloporphyin, PdC14. This is a new amphiphilic TMPyP derivative, which was developed by insertion of 14-carbon side chain and Pd^{2+} ion. The goal of this chemical modification is to increase the binding potential of PdC14 accumulation onto Gram-negative outer membrane, thereby potentially increasing the overall PDI outcome. Apart from in cancer treatment (Rapozzi et al., 2014), which showed higher cellular uptake of the C-14 substituted TMPyP and more potent photodynamic therapy against melanoma cells, no antibacterial work has been done in the literature with respect to TMPyP C-14 substitution to the best of my knowledge.

Other studies have shown that the alkylation of tetra-cationic TMPyP porphyrin derivatives improves the antimicrobial PDI outcome (Reddi et al., 2002; Xuan et al., 2019). For example, one study that evaluated the PDI antimicrobial activity against MRSA and *E. coli* of

multiple meso-substituted porphyrin compounds ranging from C6 to C22 concluded that the C10 and C14 substituted porphyrins PS produced the most bactericidal effect using white light illumination (Reddi et al., 2002). However, the PS used in this study lacked the presence of any metal at the center of the porphyrin PS molecule. Another study that compared C12 substituted porphyrin versus C12 substituted Pd-porphyrin showed that the PdC12 metalloporphyrin demonstrates improved PDI bactericidal activity against MRSA and *Candida albicans* using 415 nm blue LED light (Xuan et al., 2019). In Gram-negative *E. coli*, there was over 5 log reduction in survival fraction at 5 J/cm^2 associated with minimal 0.1 μM PdC12 dark toxicity (Xuan et al., 2019). As a result, C14 substituted metalloporphyrins as PS may offer a stronger antimicrobial PDI effect against pathogenic organisms, especially Gram-negative bacteria.

In terms of endospores, several *in vitro* studies have concluded that PDI is effective in killing *Bacillus* endospores (Demidova & Hamblin, 2005; A. Oliveira et al., 2009). For example, one study that compared *Bacillus* response to PDI using a 50 μM Toluidine blue O (TBO) dye as a PS and 40 J/cm^2 red-light irradiation showed a significant 5 log reduction in *B. cereus* spores survival rate (Demidova & Hamblin, 2005). Another study showed that using 5 μM of the cationic porphyrin derivatives 5-(4-carboxy-phenyl)-10,15,20-tris(1-methylpyridinium-4-yl)porphyrintri-iodide (Tri-Py+-Me-COOH), 10,15,20-tris(1-methylpyridinium-4-yl)-5-(pentafluorophenyl)porphy-rin tri-iodide (Tri-Py+-Me-PF), and 5,10,15,20-tetrakis(1-methylpyridinium-4-yl) porphyrin tetra-iodide (Tetra-Py+-Me) in combination with white light (400-800 nm) at an irradiance of 1690 W/m^2 results in an average of 3.5 log reduction in *B. cereus* survival rate (A. Oliveira et al., 2009). These results suggest that the newly developed lipophilic C-14 metalloporphyrin derivative would make a viable candidate for testing its effectiveness as PS against *Bacillus* endospores.

In conclusion, the newly developed ZnC14 and PdC14 offer a promising potential as a PS molecule against both Gram-positive and Gram-negative bacteria for two reasons. One is that the increased lipophilicity of this molecule would theoretically enable it to bind stronger to Gram-negative bacteria compared to ZnT4 and PdT4. Therefore, the production of ROS upon photoactivation would be closer to the targeted outer membrane structure, ultimately resulting in more potent bactericidal outcomes. For Gram-positive bacteria, the ZnC14 and the PdC14 still retains the tetra cationic charge on its structure which drives this molecule to accumulate onto the negatively charged teichoic acid composition of the peptidoglycan layer. Taken together, the PdC14 and ZnC14 are prime candidates as a PS for PDI testing not only against Gram-positive and -negative bacteria, but also against other bacterial forms such as endospores.

The trending rise in antibiotic resistance among multiple infectious organisms poses an enormous public health challenge. Infections due to resistant pathogens not only create an economical burden on individuals and healthcare systems, but also lead to increased hospitalizations and mortality rate (Marturano et al., 2019). Therefore, alternative approaches to using antibiotics such as PDI are needed.

II. HYPOTHESIS AND SPECIFIC AIMS

PDI is an alternative strategy in combating pathogenic organisms. PDI utilizes visible light, chemically developed PS, in the presence of O_2 molecules to produce ROS which kills targeted bacteria through damaging cellular membrane, proteins and DNA. The rise in antibiotic resistance and recent lack of new antibiotics development necessitate anti-microbial alternative approaches such as PDI. Cationic porphyrin derivatives have been shown to bind well with Gram-positive bacteria due to the ionic attraction between their positive charge and the negatively charged peptidoglycan layer. The addition of a long carbon chain to a porphyrin molecule increases its lipophilicity, resulting in an increased binding towards Gram-negative bacteria. However, the addition of C14 to metalloporphyrins has not yet been tested, especially against a variety of ESKAPE pathogens. The overall objective of this thesis is to specifically understand the effect of 14-carbon substituted metalloporphyrin PDI against Gram-positive and Gram-negative ESKAPE pathogens, and atypical pathogenic bacteria.

The central hypothesis of this proposal is: *The addition of C-14 side chain to metalloporphyrin enhances its binding and the photodynamic inactivation bactericidal effect against common Gram-positive and Gram-negative wound pathogens, and atypical bacteria*. To test this hypothesis the following specific aims will be addressed:

1. **To determine bacterial PS binding of C14 metalloporphyrin derivative relative to T4 metalloporphyrin derivative against both Gram-positive and Gram-negative pathogens.** The working hypothesis of this aim is: *PdC14 and ZnC14 produce stronger bacterial binding than PdT4 and ZnT4 due to improved lipophilicity.*

2. **To determine PDI antimicrobial activity of T4 and C14 metalloporphyrin derivatives against bacterial pathogens.** The working hypothesis of this aim is: *Metabolically inactive pathogens including* Bacillus cereus *endospores would be less sensitive to PDI than Gram-positive and -negative ESKAPE pathogens. Additionally, Gram positive organisms would be more susceptible to PDI than Gram-negative ESKAPE pathogens.*

CHAPTER 2: MATERIALS AND METHODS

I. Metalloporphyrins

PdT4, ZnT4, PdC14, and ZnC14 are 5,10,15,20-tetrakis(1-methylpyridinium-4-yl)-porphyrin tetra(p-toluenesulfonate) TMPyP derivatives containing either the metal palladium or zinc were prepared and obtained by Dr. Troy Skwor and Dr. Matthew Bork (Rockford University) following published procedures (Heffron et al., 2021; Skwor et al., 2016) or purchased from Frontier Scientific. Dilutions were made in sterile DI H_2O. Thermo-Scientific® Genesys 30 spectrophotometer was utilized to determine the Soret bands for all PS used in this work.

II. Light source

Battery operated 405 nm blue Quantum Light (WRAP 10®, Quantum Devices, Inc., OH, USA) portable LED as well as 430 nm blue LED device (Triton Systems, Inc.) were used as the light source for the PDI experiments throughout this research.

III. Bacterial strains and culture conditions

The following strains were obtained from the American Type Culture Collection and used for the thesis: *E. faecium* (ATCC 7171), MRSA (ATCC 43300), *P. aeruginosa* (ATCC 10145), *E. coli* (ATCC 11775), clinical *E. coli* WDL-149 was provided by Wisconsin Diagnostics lab (an ESBL-producing multi-drug resistant strain acquired from a pressure ulcer), *Bacillus cereus* (ATCC 10876), and *A. baumannii* (ATCC 19606). Frozen pure stocks of these bacterial strains had already been made and were stored in the -80 ˚C freezer in 1.5 ml cryogenic vials. Using aseptic technique, these strains were inoculated into sterile test tubes containing either Luria broth (LB) or Tryptic Soy Broth (TSB) depending on the experiment objective. Negative controls were also performed to ensure no contamination of the broth media used, or

during the inoculation procedure had occurred. The bacteria inoculated broths were then incubated overnight in a shaker incubator at 35 ˚C and 150 rotations per minute (RPM) for approximately 24 hours. The bacterial cells were harvested the following day using centrifugation at 7,000 x g for 5 minutes, then resuspended in 1x phosphate buffer saline (PBS). A 0.5 McFarland Standard suspension was made using sterile 1x PBS as a diluent until the optical density (OD600) of 0.08 – 0.1 was obtained, which corresponds to approximately $1.5*10^8$ colony forming units per milliliter (CFUs/ml).

IV. Endospore purification

Bacillus cereus (ATCC 10876) (BSL-2) was utilized for studying PDI effects on endospores. To obtain *Bacillus* endospores, a sporulation medium was made following published procedures (Banerjee et al., 2012; Demidova & Hamblin, 2005). The sporulation medium consisted of 8 g nutrient broth (Ward's Science), 1 g KCl, and 0.25 g $MgSO_4$ per 500 ml DI (de-ionized) H_2O. The pH was then adjusted to 7.0, and the medium was autoclaved and cooled down. Subsequently, filter-sterilized 0.5 ml of 1 M $Ca_2(NO_3)_2$, 0.5 ml of 0.1 M $MnCl_2$, 0.5 ml of 1 mM $FeSO_4$, and 1 ml of 50% (w/v) glucose were added to the autoclaved 500 ml sporulation medium. Frozen *Bacillus* pure stock at – 80°C was inoculated into 250 ml sporulation medium and incubated in a shaker at 37° C and 150 rpm for at least three days. The culture was observed periodically for endospore purity using malachite green staining following published procedure (Hamouda et al., 2002), and was taken out of the incubator once >90% spore purity was achieved. The 250 ml spore containing culture was then centrifuged (Avanti® J-E, JA-20 rotor) at 4,000 x g and 4° C for 10 minutes. The pellet was resuspended in cold sterile water (Milli-pore), washed multiple times in sterile water, and heated in 80°C water bath for 20 minutes until >99%

spore purity was obtained, with the remaining material being fragments of vegetative cells. The spore suspension was then stored at 4° C until used.

V. PS Uptake studies

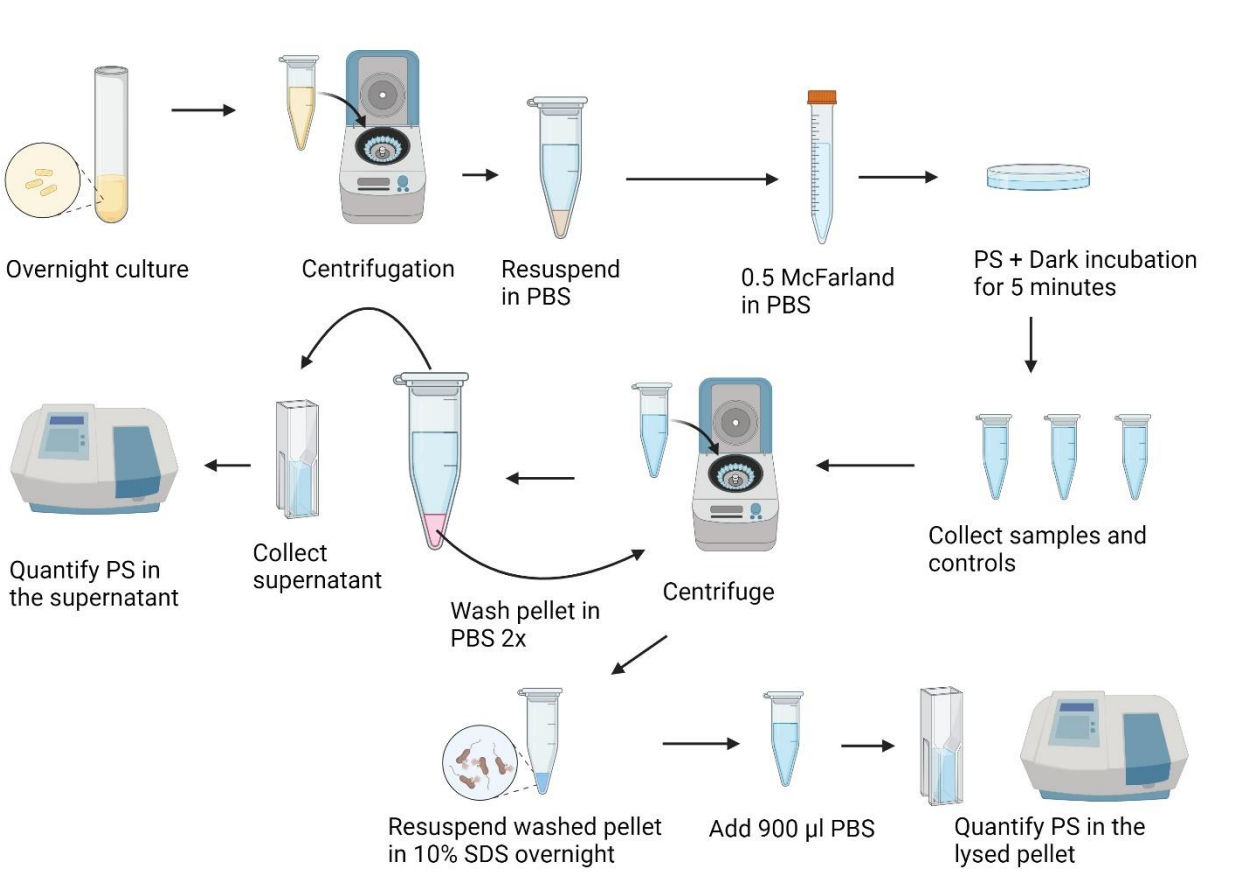

Figure 1: Visual illustration of PS bacterial binding experiments.

For the porphyrin uptake studies (Figure 1), the bacterial 0.5 McFarland suspension was incubated with 1 µM PdT4 or 1 µM PdC14 photosensitizers in the dark for 5 minutes. Controls included 1 µM PdT4 in PBS, 1 µM PdC14 in PBS, untreated *E. faecium*, and untreated *A. baumannii* suspensions. Following PS incubation, the cells were centrifuged at 10,000 RPM for 10 minutes, the supernatant absorbance was measured across a range of 360-750 nm to determine the unabsorbed portion of the PS relative to the positive control. Then, the pellets were resuspended in 1x PBS, and two washes were performed to eliminate any unbound or loosely

bound PS. Subsequently, the bacterial pellets were lysed overnight in 100 µl 10% Sodium Dodecyl Sulfate (SDS) and resuspended in 900 µl PBS as described previously (Sułek et al., 2020). Controls included 10% SDS in PBS, untreated *E. faecium* lysate, and untreated *A. baumannii* lysate. Same as the supernatant, the absorbance was measured across a spectrum range of 360-750 nm to determine the absorbed/bound portion of the PS used in the study.

VI. Photodynamic inactivation

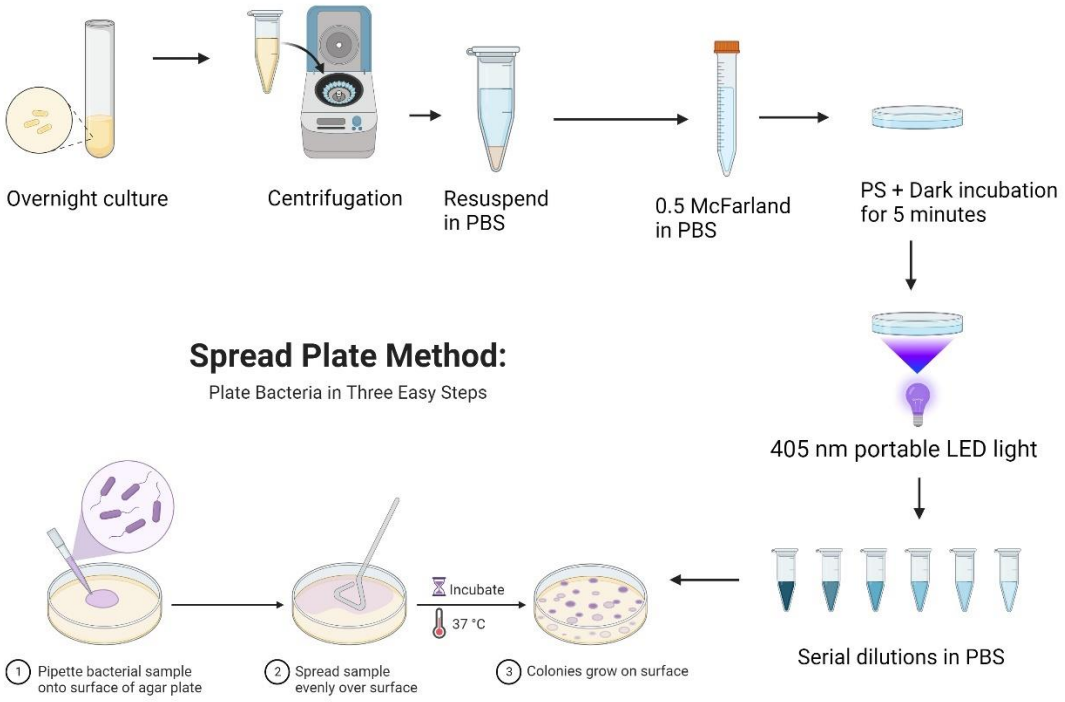

Figure 2: Visual illustration of PDI experiments.

Bacterial overnight cultures were pelleted at 10,000 rotations per minute (rpm) which corresponds to 9,193 x g force. The supernatant was discarded in 10% bleach and the cells were resuspended in 1 ml PBS. Subsequently, the resuspended stock cells were used to make the 0.5 McFarland standard using a sterile PBS with an OD600 of 0.08-0.1 absorbance value. Two ml of the adjusted bacterial suspension was then added to 35 mm incubation plates per irradiance used.

The porphyrin was then added and allowed to incubate with the suspension for 5 minutes in the dark (Figure 2). A negative control plate was utilized where equivalent porphyrin was added to PBS only (without cells) and incubated in the dark for 5 minutes as well. The 405 nm or 430 nm blue LED light was used in irradiances ranging between 0.08-5 J/cm^2 to determine the bactericidal ability of ZnT4, ZnC14, PdT4, and PdC14 metalloporphyrin derivatives in combination with light across targeted pathogens. After PDI treatment, serial dilutions in 1x PBS were made up to 1:100,000. Then, 15 µl was aseptically inoculated on 60 x 15 mm TSA plates and incubated at 37° C for 24 hours (Figure 2). The colonies were counted, and log inactivation was determined relative to untreated control CFU numbers. CFU/ml was determined using the equation [CFU/mL = (CFU x dilution factor) ÷ volume plated], while log inactivation was determined using [Untreated CFU/ml ÷ Treated CFU/ml].

For the endospore PDI experiments, the spore stock was serially diluted until 1*10^7 colony forming units/ml (CFUs/ml) was obtained. The spores were then incubated in the dark with 3 µM ZnC14 over a range of 5 minutes to 3 hours. Subsequently, light irradiance of 4.4 J/cm^2 was applied to each treatment group and 15 µl was aseptically plated on TSA plates which were then incubated at 30° C for 24 hours. Next, colonies were counted, and log inactivation was determined using the same method described earlier.

VII. Statistical analysis

The data obtained from our PDI experiments were analyzed using GraphPad Prism. Significance between treatment groups of our PDI experiments used the analysis of variance test. Two-way ANOVA was used to analyze the CFU/ml and log inactivation means between and within treatment groups. This was followed by Tukey's multiple comparison test to determine significant differences between PDI treatments. An unpaired t-test was also used for the MRSA

PdC14 treatment relative to the control. Data collected were identified as significant when $P < 0.05$.

CHAPTER 3: RESULTS

Specific Aim I:

First, we needed to test our hypothesis that PdC14 metalloporphyrin has a stronger bacterial binding profile over PdT4. Therefore, we incubated 10 µM PdC14 and 10 µM PdT4 with a Gram-negative representative of the ESKAPE pathogens, *A. baumannii*.

Upon 5 minutes incubation in dark conditions, the suspensions were centrifuged and washed two times with PBS to remove unbound/loosely bound porphyrin. To determine the bound versus the non-bound portion of the two metalloporphyrin derivatives, we initially measured the supernatants using spectrophotometry across a range from 360-700 nm. Subsequently, we lysed the bacteria cells in 10% SDS after two PBS washes similarly. In addition, 10 µM of both metalloporphyrin derivatives were utilized in 1x PBS as positive controls.

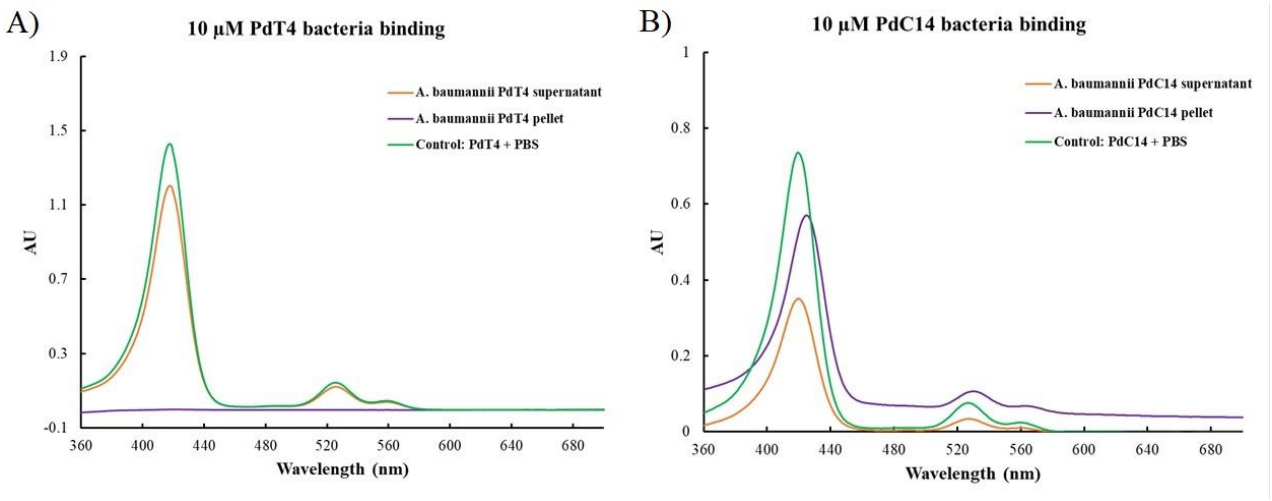

Figure 3: Binding abilities of palladium-porphyrin to *A. baumannii*. The bacteria were incubated with the corresponding PS for 5 minutes in a dark environment. Subsequently, the PS was quantified in both the supernatants and the pellets to determine bacterial binding using spectrophotometry. A) 10 µM PdT4 absorbance spectrum in *A. baumannii* supernatant and pellet. B) 10 µM PdC14 absorbance spectrum in *A. baumannii* supernatant and pellet.

Porphyrin can either be found in the bacterial supernatant or bound to bacteria and therefore in the pellet. Stronger binding will be evident with greater absorbance value unit (A.U.) of the Soret peak within the pellet sample. The results of 10 µM PdT4 metalloporphyrin showed that the supernatant of *A. baumannii* contains 84.27% of the PS relative to the PdT4 positive control (Fig. 3A: 1.205 vs 1.43 respectively). Additionally, the lysed pellets of *A. baumannii* shows a flat absorbance spectrum with no Soret peak detected identifying the bacterial pellets did not retain the PdT4 metalloporphyrin (Figure 3A: 0.001 vs 1.43 respectively). The 10 µM PdC14, on the other hand, revealed a higher quantity of the PdC14 in the *A. baumannii* pellet comprising 77.2% of total porphyrin added (Figure 3B: 0.569 vs 0.737) supporting our hypothesis that the addition of an alkyl side chain to the PdT4 does indeed improve the bacterial binding ability of the PS.

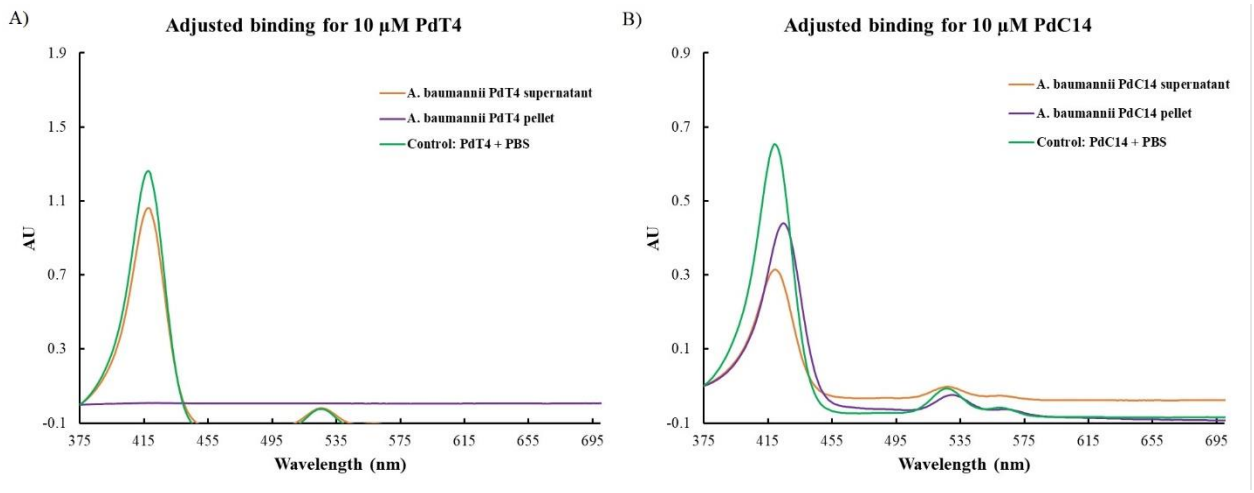

Figure 4: Adjusted palladium-porphyrin binding to *A. baumannii*. All absorbance values were modified after zeroing the A.U. at 375 nm. This adjustment was performed to optimize the graph to enable to analyze multiple absorbance spectrums. A) Adjusted 10 µM PdT4 absorbance spectrum in *A. baumannii* supernatant and pellet. B) Adjusted 10 µM PdC14 absorbance spectrum in *A. baumannii* supernatant and pellet.

Upon adjusting the absorbance values to zero values at 375 nm, the results remained the same whereby the 10 µM PdT4 derivative demonstrated poor bacterial binding ability detected in the pellet relative to the control (Figure 4A: 0.01 vs 1.263) reflecting 0.79% binding (Figure 4A and table 1). PdC14 on the other hand, displayed a superior binding profile to *A. baumannii* as shown by the presence of the Soret peak (Figure 4B: 0.439 vs 0.654) accounting for 67% of total porphyrin found withing the bacterial pellet (Figure 4B and Table 1).

Porphyrin	Concentration	Organism	Peak AU	Adjusted peak AU	wavelength	Type	Porphyrin-bacteria Binding %	Adjusted Binding %
PdT4	10 µM	Control	1.43	1.263	418 nm	N/A	N/A	N/A
		A. baumannii	1.205	1.062	418 nm	Supernatant	0.07%	0.79%
			0.001	0.01		Pellet		
PdC14		Control	0.737	0.654	419 nm	N/A	N/A	N/A
		A. baumannii	0.351	0.315	419 nm	Supernatant	77%	67%
			0.569	0.439	424 nm	Pellet		

Table 1. Palladium-porphyrin bacterial binding to *A. baumannii* summary. Spectrophotometry data obtained from both 10 µM metalloporphyrin derivatives binding experiment in *A. baumannii*. The binding percentages were calculated via dividing the Soret peak AU value of the pellet by the Soret peak AU of the corresponding positive control in each PS used.

It is also noted that the PdC14 *A. baumannii* pellet Soret peak was shifted to 424 nm wavelength (Table 1), further suggesting that binding of PdC14 to bacterial cell components occurred. Taken together, these results illustrate that the addition of a C-14 side chain to PdT4 improves the ability of the PS to bind to Gram-negative *A. baumannii* which supports the hypothesis of the first specific aim.

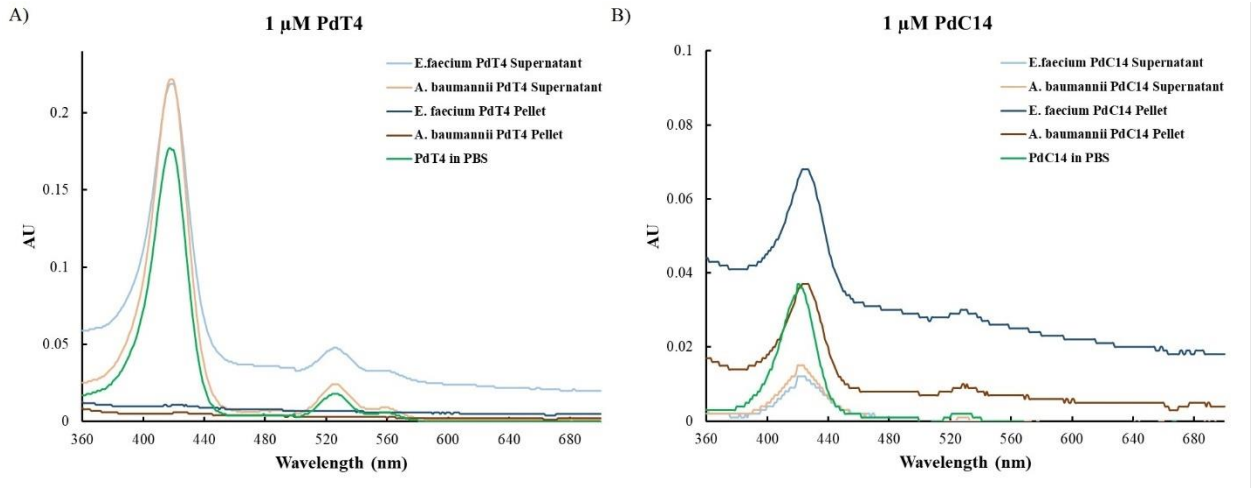

Figure 5: Palladium-porphyrin binding comparison to *E. faecium* and *A. baumannii*. The bacteria were incubated with the corresponding PS for 5 minutes in a dark environment. Subsequently, the PS was quantified in both the supernatants and the pellets of each organism to determine bacterial binding using spectrophotometry. A) 1 µM PdT4 absorbance spectrum in *E. faecium* and *A. baumannii* supernatant and pellet. B) 1 µM PdC14 absorbance spectrum in *E. faecium* and *A. baumannii* supernatant and pellet.

Next, we were interested to know if a similar binding pattern to the 10 µM PS would still occur at 1:10 of PS the concentration. Therefore, we tested 1 µM PdT4 and 1 µM PdC14 metalloporphyrin derivatives in both Gram-positive *E. faecium* and Gram-negative *A. baumannii*. As expected, the PdT4 Soret peak was only detected in the supernatant (A.U. = 0.219 in *E. faecium* and A.U. = 0.222 in *A. baumannii*) and a weak Soret peak was detected in both bacterial pellets (Figure 5A: A.U. = 0.011 in *E. faecium* and A.U. = 0.006 in *A. baumannii*). The PdT4 positive control A. U. was recorded at 418 nm with a value of 0.177 (Figure 5A). Conversely, PdC14 Soret peaks were detected in both bacterial pellets with A.U. values of 0.068 and 0.037 in *E. faecium* and *A. baumannii* respectively (Figure 5B), as well as a red shift of the Soret peak indicative of successful bacterial binding of PdC14. The PdC14 positive control was recorded at 420 nm wavelength with an A.U. value of 0.037 (Figure 5B).

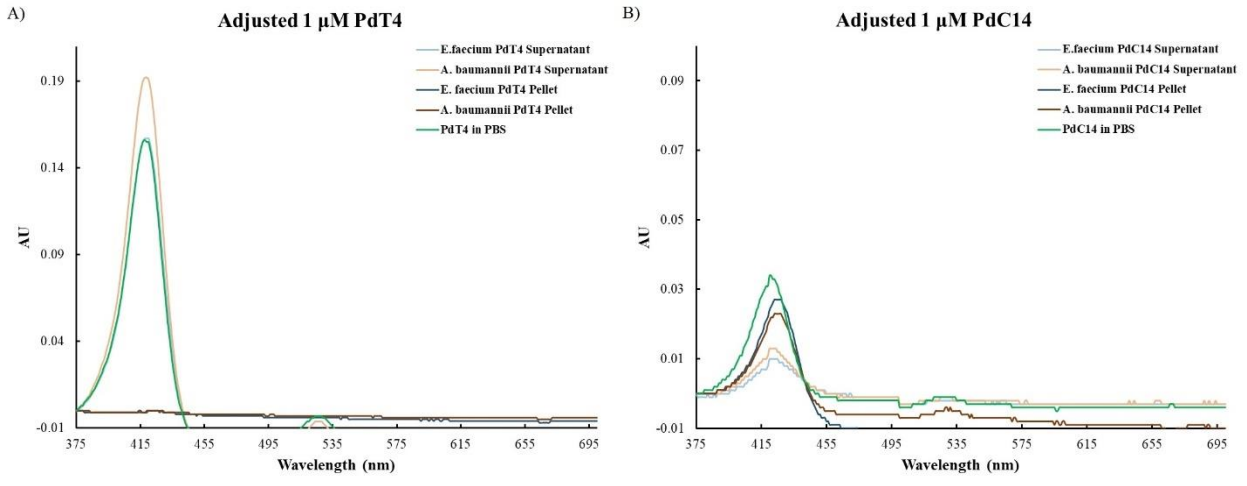

Figure 6: Adjusted palladium-porphyrin binding comparison to *E. faecium* and *A. baumannii*. All absorbance values were modified after zeroing the A.U. at 375 nm. This adjustment was performed to optimize the graph to enable to analyze multiple absorbance spectrums. A) 1 µM PdT4 absorbance spectrum in *E. faecium* and *A. baumannii* supernatant and pellet. B) 1 µM PdC14 absorbance spectrum in *E. faecium* and *A. baumannii* supernatant and pellet.

After zeroing the absorbance value at 375nm and adjusting the rest of the absorbance spectrum values, both the *E. faecium* (A.U. = 0.157) and *A. baumannii* (A.U. = 0.192) PdT4 supernatant still show a highly similar Soret peak to that of the positive control (A.U. = 156), suggesting no binding did occur (Figure 6A). In addition, the pellets show adjusted A.U. value of 0 in both bacteria (Figure 6A).

As for the 1 µM PdC14, both *E. faecium* and *A. baumannii* show higher pellet peaks compared to their supernatant's suggesting that the bacterial cells bound most of the metalloporphyrin (Figure 6B and Table 2). For the PdC14 adjusted spectrum, *E. faecium* and *A. baumannii* supernatant contained 29.41% and 38% of the total porphyrin (Figure 6B: 0.01 and 0.013 respectively). The total PdC14 detected in the pellets of *E. faecium* and *A. baumannii* was 79.41% and 67.65% respectively (Figure 6B: 0.027 in *E.faecium* and 0.023 in *A.baumannii*).

Porphyrin	Concentration	Organism	Peak AU	Adjusted peak AU	wavelength	Type	Porphyrin-bacteria Binding %	Adjusted Binding %
PdT4	1 µM	Control	0.177	0.156	418 nm	N/A	N/A	N/A
		E. faecium	0.219	0.157	418 nm	Supernatant	6%	0%
			0.011	0		Pellet		
		A. baumannii	0.222	0.192	420 nm	Supernatant	3%	0%
			0.006	0		Pellet		
PdC14		Control	0.037	0.034	420 nm	N/A	N/A	N/A
		E. faecium	0.012	0.01	420 nm	Supernatant	184%	79%
			0.068	0.027		Pellet		
		A. baumannii	0.015	0.013	423 nm	Supernatant	100%	68%
			0.037	0.023		Pellet		

Table 2. Palladium-porphyrin ESKAPE bacterial binding summary. Spectrophotometry data obtained from both 1 µM metalloporphyrin derivatives binding experiment in *E. faecium* and *A. baumannii*. The binding percentages were calculated via dividing the Soret peak AU value of the pellet or supernatant by the Soret peak A.U. of the corresponding positive control in each PS used.

Overall, these data support our hypothesis that the increase in C14 bacterial binding compared to T4 in both Gram-positive and Gram-negative bacteria occurs at 1 µM concentration as well (Figures 5 and 6 and Table 2).

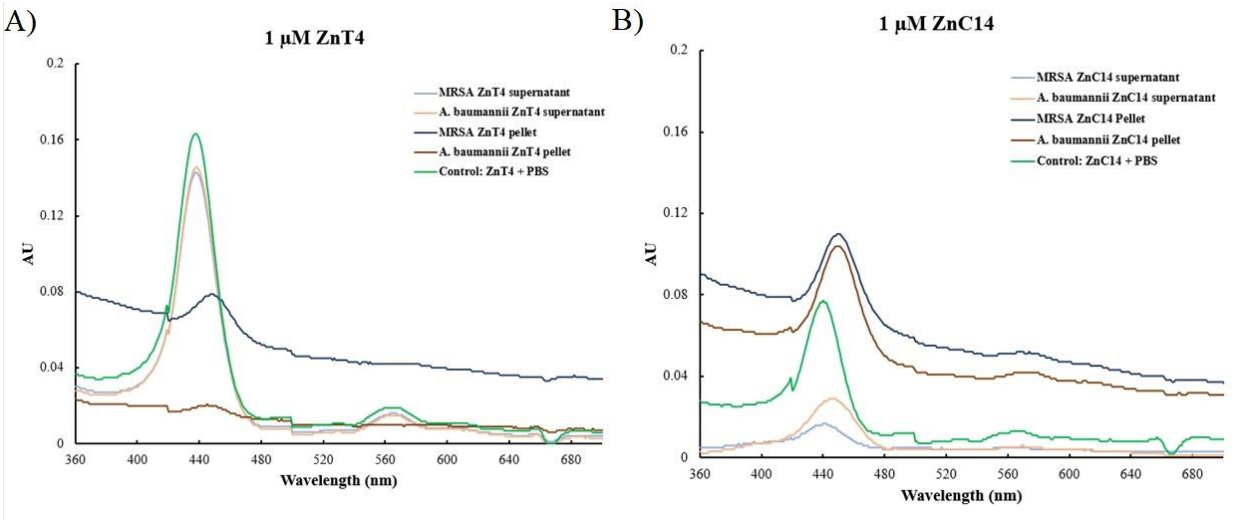

Figure 7: Zinc-porphyrin binding comparison to MRSA and *A. baumannii*. The bacteria were incubated with the corresponding PS for 5 minutes in a dark environment. Subsequently, the PS was quantified in both the supernatants and the pellets of each organism to determine bacterial binding using spectrophotometry. A) 1 µM ZnT4 absorbance spectrum in MRSA and *A. baumannii* supernatant and pellet. B) 1 µM ZnC14 absorbance spectrum in MRSA and *A. baumannii* supernatant and pellet.

In ZnT4 metalloporphyrin unsubstituted derivative, the Soret peaks were highly evident in the supernatant of the PS incubated bacterial suspension (Figure 7A). In the ZnT4, both MRSA as well as *A. baumannii* show high amount of the total ZnT4 in the supernatant with 87.7% and 89.57% detected (Figure 7A: 0.143 and 0.146 respectively). Alternatively, most of ZnC14 was detected in the pellets in comparison to the supernatants of both MRSA and *A. baumannii* representing 49% and 80% of the total ZnC14 porphyrin upon adjust the absorbance (Figure 8B: 0.025 and 0.041 respectively). In conclusion, the Zn-metalloporphyrin shows similar binding improvement with the C14 alkylation (Figures 7 and 8 and Table 3). Overall, the results are consistent with our hypothesis as well as with our prior findings (Figures 3 - 6 and Tables 1 and 2).

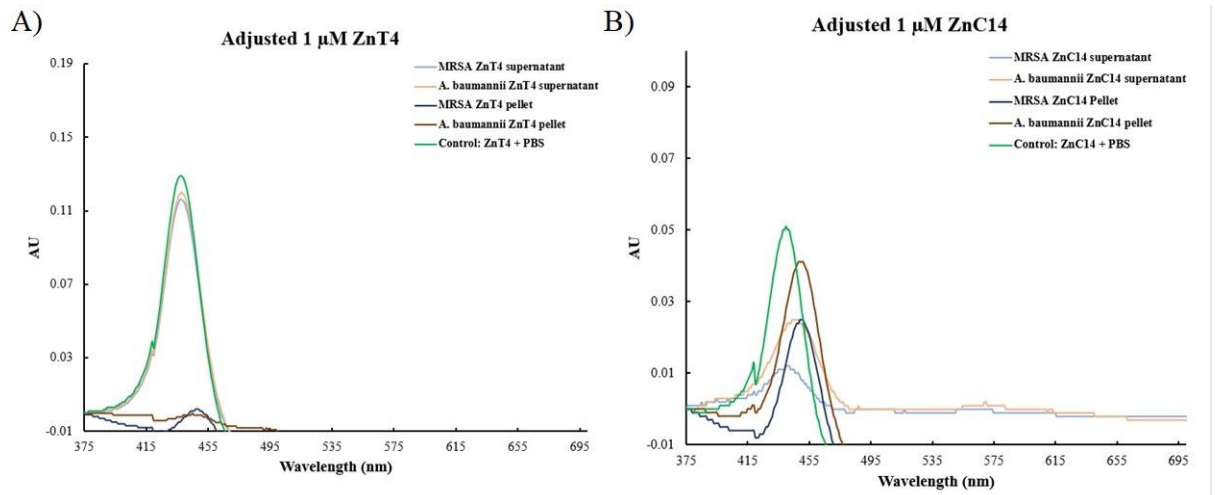

Figure 8: Adjusted zinc-porphyrin binding comparison to MRSA and *A. baumannii*. All absorbance values were modified after zeroing the A.U. at 375 nm. This adjustment was performed to optimize the graph to enable to analyze multiple absorbance spectrums. A) Adjusted 1 µM PdT4 absorbance spectrum in MRSA and *A. baumannii* supernatant and pellet. B) Adjusted 1 µM PdC14 absorbance spectrum in MRSA and *A. baumannii* supernatant and pellet.

Porphyrin	Concentration	Organism	Peak AU	Adjusted peak AU	wavelength	Type	Porphyrin-bacteria Binding %	Adjusted Binding %
ZnT4	1 µM	Control	0.163	0.129	438 nm	N/A	N/A	N/A
		MRSA	0.143	0.116	438 nm	Supernatant	48%	2%
			0.079	0.002	448 nm	Pellet		
		A. baumannii	0.146	0.12	438 nm	Supernatant	13%	0%
			0.021	0	445 nm	Pellet		
ZnC14		Control	0.077	0.051	440 nm	N/A	N/A	N/A
		MRSA	0.017	0.012	440 nm	Supernatant	143%	49%
			0.11	0.025	449 nm	Pellet		
		A. baumannii	0.029	0.025	444 nm	Supernatant	135%	80%
			0.104	0.041	448 nm	Pellet		

Table 3. Zinc-porphyrin ESKAPE bacterial binding summary. Spectrophotometry data obtained from both 1 µM metalloporphyrin derivatives binding experiment in MRSA and *A. baumannii*. The binding percentages were calculated via dividing the Soret peak AU value of the pellet by the Soret peak AU of the corresponding positive control in each PS used.

In summary, all these results support each other, our hypothesis, and further confirm that the improved bacterial binding profile is attributable to the addition of the C-14 to the metalloporphyrin regardless of the metalloporphyrin concentration used or the metal incorporated at the center of the PS molecule. Taken together, the addition of a lipophilic alkyl chain to metalloporphyrin improves the tetra cationic TMPyP PS ability to bind to bacterial cells in Gram-positive and Gram-negative ESKAPE pathogens.

Specific Aim II:

I. PDI bactericidal comparison between T4 and C14 metalloporphyrin derivatives in Gram-positive and Gram-negative bacteria:

Having concluded in specific aim 1 that PdC14 and ZnC14 derivatives have an improved bacterial binding profile compared to PdT4 and ZnT4 in both Gram-positive and Gram-negative bacterial pathogens, here we opted to evaluate the PDI antimicrobial activity between the two derivatives against Gram-positive and Gram-negative organisms. PDI primarily relies on generating bactericidal ROS once PSs get activated by light. This process requires an optimized wavelength selection that excites the PS at its Soret peak to deliver the highest ROS ratio thereby increasing the bacterial cytotoxic effect. As a result, we compared T4 versus C14 metalloporphyrin PDI as follows:

1. Concentration effect of metalloporphyrin PDI on bactericidal effect:

First, we aimed to evaluate both metalloporphyrin derivatives PDI antimicrobial activity against Gram-negative *A. baumannii*. In our previous publication, 10 μM metalloporphyrin concentration was utilized to evaluate the metalloporphyrin antimicrobial activity (Skwor et al., 2016). In addition, the ZnT4 and ZnC14 Soret peaks are slightly red shifted at 438 and 440 nm wavelength respectively (Table 3), therefore, a newly acquired 430 nm LED light was utilized to

excite the ZnT4 and ZnC14 metalloporphyrin derivatives for PDI antimicrobial analysis. Conversely, 405 nm portable LED was used to assess PdT4 and PdC14 PDI, which have Soret peaks at 418 and 420 nm respectively. To compare the T4 versus the C14 PS PDI antimicrobial activity, we tested incubating *A. baumannii* with 1 and 10 μM ZnT4 and ZnC14 as well as MRSA with 0.1 and 1 μM ZnC14 to determine if a lower concentration of the C14 substituted metalloporphyrin can achieve the desired antimicrobial activity for our subsequent PDI investigations.

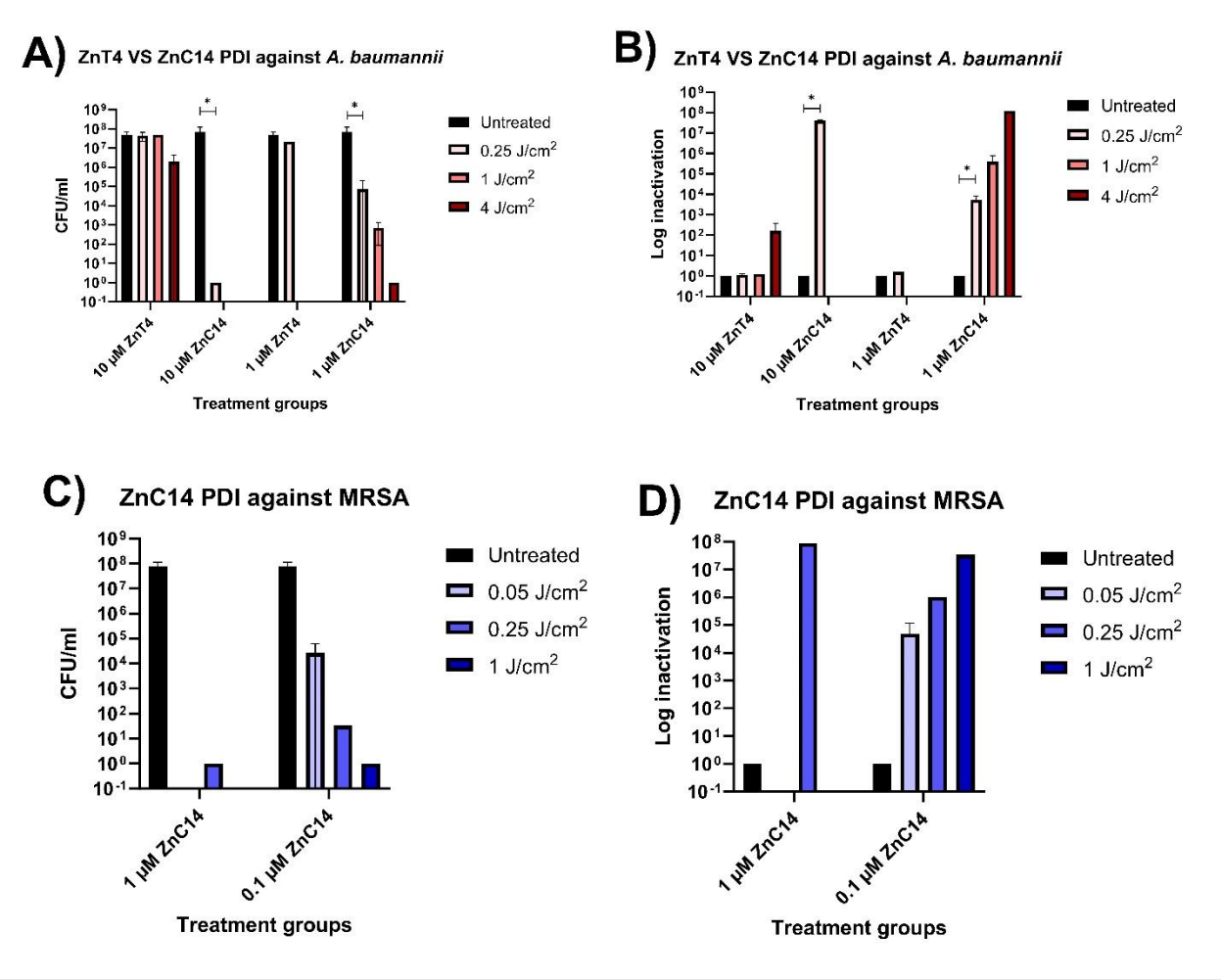

Figure 9: 430 nm PDI using ZnT4 and ZnC14 against *A. baumannii* and MRSA. The bacteria were incubated with the corresponding metalloporphyrin for 5 minutes in a dark environment. Then exposed to 430 nm LED light at multiple irradiances. A) *A. baumannii* PDI comparison in CFU/ml. B) *A. baumannii* PDI comparison in log inactivation. C) MRSA PDI comparison in CFU/ml. D) MRSA PDI comparison in log inactivation. Each bar represents 3 or less independent experiments. * $P < 0.05$

The results show that 10 µM ZnC14 at 0.25 J/cm^2 had an excellent PDI bactericidal potency whereby all *A. baumannii* bacterial cells were fully killed compared to the ZnT4 PDI which only showed 1.22E+00 log inactivation at the same irradiance, corresponding to 9.74% killing rate (Figure 9A and 9B). Additionally, all *A. baumannii* bacterial cells have been fully

inactivated at 4 J/cm^2 using 1 μM ZnC14 (Figure 9A and 9B). It is worth noting that only 0.25 J/cm^2 irradiance represents 3-independent experiments in both 1 and 10 μM ZnC14. Therefore, we carried out unpaired t-test statistical analysis to determine if the difference between 0.25 J/cm^2 and the untreated group is significant. The results indicate statistically significant differences in both 1 and 10 μM ZnC14 relative to the untreated control with *P*-value = 0.008 for both concentrations (Figure 9A). Also, statistically significant results were found in log inactivation between the untreated and 0.25 J/cm^2 groups in both 1 and 10 μM ZnC14 with *P*-value = 0.015 and *P*-value = 0.004 respectively (Figure 9B).

Considering it worked so well against a Gram-negative bacterium, we next wanted to test ZnC14 against a Gram-positive bacterium. 430 nm PDI using 1 μM ZnC14 at 0.25 J/cm^2 against MRSA showed full inactivation (Figure 9C and 9D) whereby 1 J/cm^2 irradiance was needed to achieved the same outcome using 1:10 the concentration at 0.1 μM ZnC14 (Figure 9C and 9D). Unfortunately, there is no ZnT4 data to show regarding MRSA PDI. In addition, MRSA data were representative of one or two independent experiments. As a result, we were unable to run statistical analysis. Overall, the C14 substituted metalloporphyrin shows a strong PDI antimicrobial activity. Therefore, we decided to continue our analysis using 1 μM to further evaluate the C14 substituted metalloporphyrin against Gram-positive and Gram-negative bacterial pathogens.

2. <u>C14 alkylation improves PDI response regardless of the incorporated metal within porphyrin:</u>

Next, we were interested in understanding if the C14 substitution would improve the PDI antimicrobial activity relative to the unsubstituted T4 regardless of the metal incorporated at the

center of the metalloporphyrin molecule. Therefore, we compared the *A. baumannii* log inactivation using PdT4, PdC14, ZnT4, and ZnC14 metalloporphyrin derivatives.

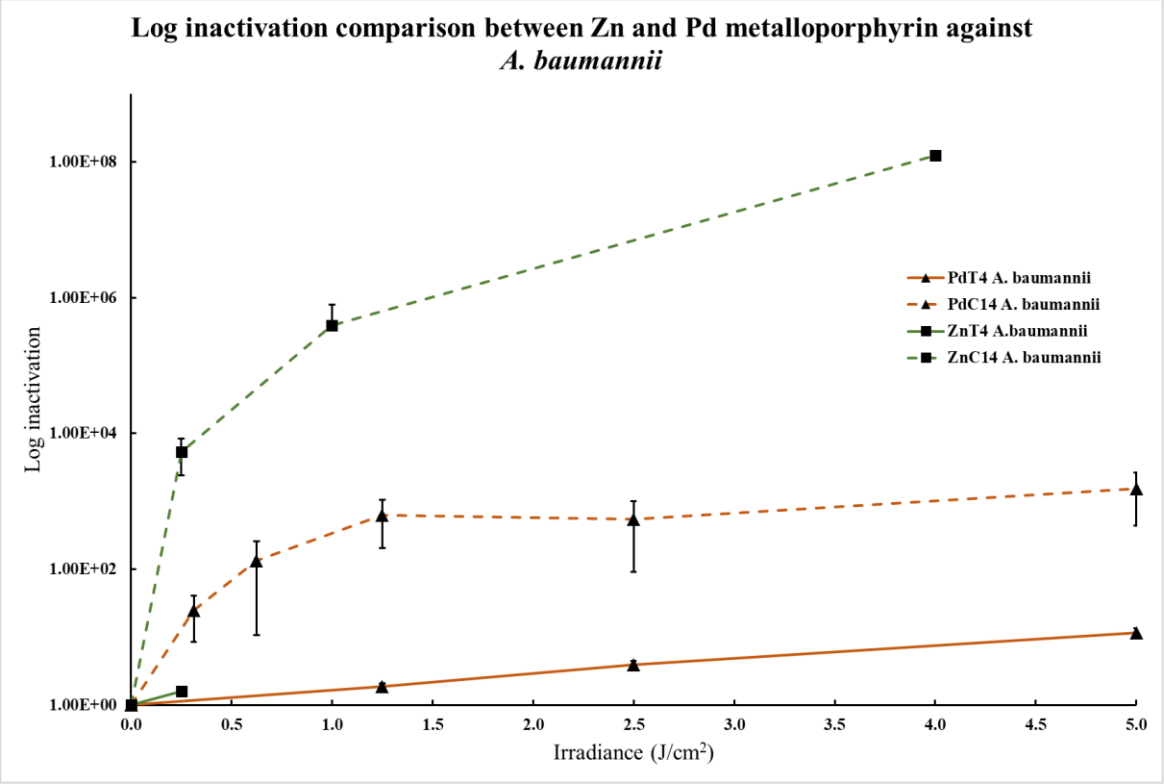

Figure 10: Comparison of metalloporphyrins with blue light PDI against *A. baumannii*. The bacteria were incubated with the corresponding metalloporphyrin for 5 minutes in a dark environment, then exposed to LED light at multiple irradiances. The dashed line represents the C14 PDI results while the straight light showcases T4 metalloporphyrin PDI. Green line: ZnT4 and ZnC14 PDI results. Brown line: PdT4 and PdC14 PDI results. All experiments were performed using 1 μM PS concentration. Data represents 3 or less independent experiments with duplicates per experiment.

The results show that the addition of C14 improves the bactericidal PDI outcome in both metals (Pd and Zn) relative to the unsubstituted T4 (Figure 10). Although we are missing higher than 0.25 J/cm^2 irradiance data for the 1 μM ZnT4 against *A. baumannii*, no more than 1.65E+02 log inactivation at 4 J/cm^2 was achieved (96.06% killing rate), using 10 μM of the same metalloporphyrin (Figure 9A). Regardless, at 0.25 J/cm^2 irradiance, 1 μM ZnC14 shows

5.36E+03 log inactivation (99.9% reduction in survival fraction) whereas ZnT4 only shows 1.58E+00 log inactivation (55.76% reduction in survival fraction) (Figure 10).

The PdC14 PDI also shows enhanced log inactivation of *A. baumannii* compared to PdT4 by no less than 2 logs (99% more reduction) across all three irradiances 1.25, 2.5 and 5 J/cm^2 (Figure 10).

In conclusion, the addition of C14 alkyl side chain shows enhanced antimicrobial PDI activity with both metals, palladium and zinc, suggesting that this improvement can occur regardless of which metal is incorporated at the center of metalloporphyrin derivatives.

3. Determining PdT4 versus PdC14 PDI bactericidal effect against Gram-positive and Gram-negative ESKAPE pathogens:

Next, we aimed to evaluate both PdT4 and PdC14 at 1 μM concentration against *E. faecium* as a Gram-positive representative of the ESKAPE pathogens and *A. baumannii* as a Gram-negative representative of the ESKAPE pathogens using 405 nm LED light. Therefore, we incubated the targeted bacterial suspensions with both corresponding metalloporphyrin for 5 minutes in the dark. Then, we exposed the suspensions to LED light at multiple irradiances to determine CFUs/ml and log inactivation.

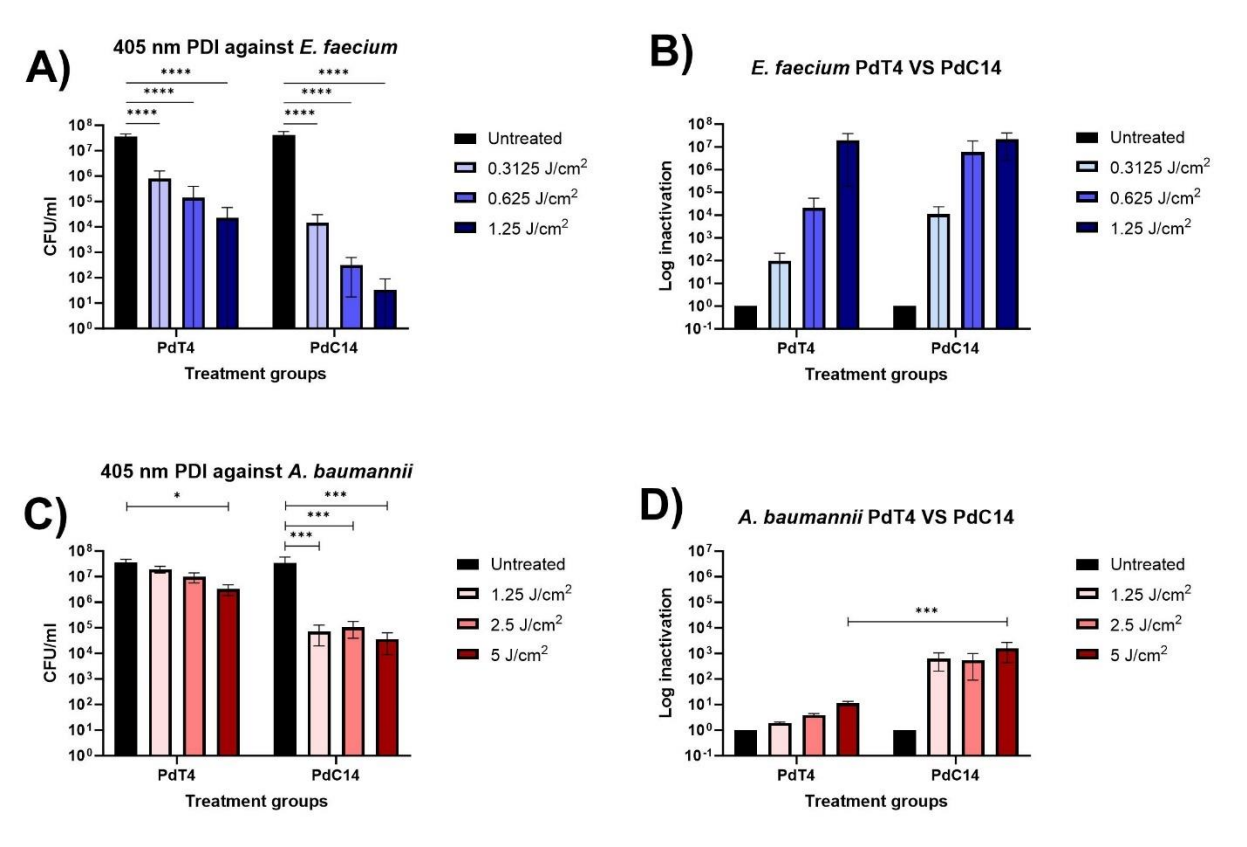

Figure 11: PDI comparison between PdT4 and PdC14 against *E. faecium* and *A. baumannii*. Bacterial suspensions were incubated for 5 minutes in a dark environment with either PdT4 or PdC14. Then, exposed to 405 nm LED light at multiple irradiances. Untreated control is represented as 0 J/cm^2. Dashed line: PdT4 incubated bacteria. Straight line: PdC14 incubated bacteria. The purple color represents *E. faecium*, with darker color intensity corresponding to higher irradiance while the red color represents *A. baumannii* with darker color intensity corresponding to higher irradiance. A) and B) PDI outcome in CFU/ml. C) and D) PDI outcome in log inactivation. Each irradiance represents the average of at least in 3-independent performed experiments with duplicate per experiment. * $P \leq 0.05$, *** $P \leq 0.0005$.

In Gram-positive *E. faecium*, the results showed 9.69E+01 log inactivation (97.82% cell reduction) at 0.3215 J/cm^2 for the PdT4 whereas 1.09E+04 log inactivation (99.96% killing rate) was achieved with PdC14 at the same irradiance (Figure 11A and 11B). At 0.625 J/cm^2, PdC14 shows 6.06E+06 log inactivation, corresponding to 99.999% killing rate, whereas PdT4 shows 2.13E+04 log inactivation, corresponding to 99.61% killing rate, in comparison (Figure 11A and

11B). Lastly, PdT4 shows 1.93E+07 log inactivation at 1.25 J/cm^2 irradiance treatment, corresponding to 99.9999% killing rate, while PdC14 shows 2.19E+07 log inactivation corresponding to 99.9999% killing rate (Figure 11A and 11B). In summary, this shows that *E. faecium* has a lower survival rate with PdC14 PDI than with PdT4 PDI up until the 1.25 J/cm^2 irradiance where both produce about 7 log inactivation. Therefore, the addition of C14 alkyl chain improves PDI outcome against Gram-positive *E. faecium*. Two-way ANOVA analysis indicated statistically significant results for each irradiance treatment against the untreated control ($P < 0.0001$).

In Gram-negative *A. baumannii*, the results overall showed that Gram-negative bacterial pathogens are less susceptible to PDI treatment than Gram-positive organisms (Figure 11). For example, with both metalloporphyrin derivatives, PdT4 and PdC14, higher irradiance dosages were required compared to Gram-positive *E. faecium* (Figure 11). Nevertheless, PdC14 still shows improvement over PdT4. For example, at 1.25 J/cm^2, PdT4 PDI shows 1.88E+00 log inactivation (46.67% killing rate) whereas PdC14 PDI shows 6.31E+02 log reduction in comparison, accounting for 99.77% killing rate (Figure 11C and 11D). At 5 J/cm^2 irradiance, PdT4 PDI was only able to achieve 1.15E+01 log inactivation, corresponding to 90.97% reduction in survival fraction, whereas PdC14 PDI shows an improved antimicrobial activity with 1.55E+03 log inactivation, corresponding to 99.88% killing rate (Figure 11C and 11D). PdC14 demonstrates an enhanced PDI bactericidal effect relative to PdT4 against Gram-negative *A. baumannii*. Two-way ANOVA analysis indicated no statistically significant differences were found in PdT4 1.25 and 2.5 J/cm^2 treatment groups relative to the untreated ($P > 0.05$). However, in the 5 J/cm^2 group relative to the untreated, there was a statistically significant difference ($P <$

0.05). Additionally, statistically significant results were found between PdT4 and PdC14 treatment groups at 5 J/cm^2 ($P < 0.05$) (Figure 11D).

Lastly, although the addition of C14 to the unsubstituted PdT4 shows improvement in the antimicrobial PDI outcome against both Gram-positive and Gram-negative ESKAPE pathogens we tested, Gram-negative *A. baumannii* still exhibited less susceptibility than Gram-positive *E. faecium* against PDI.

4. Determining TSB VS LB growth media effects on PDI response:

One of the challenges we faced during our PDI investigation was that *E. faecium* overnight growth using LB was limited. Specifically, the visual turbidity of LB when inoculated with *E. faecium* was significantly less than with any other inoculated organism used during our experiments. Furthermore, *E. faecium* overnight looks significantly more turbid when grown in TSB compared to when the organism is grown in LB (Figure 12).

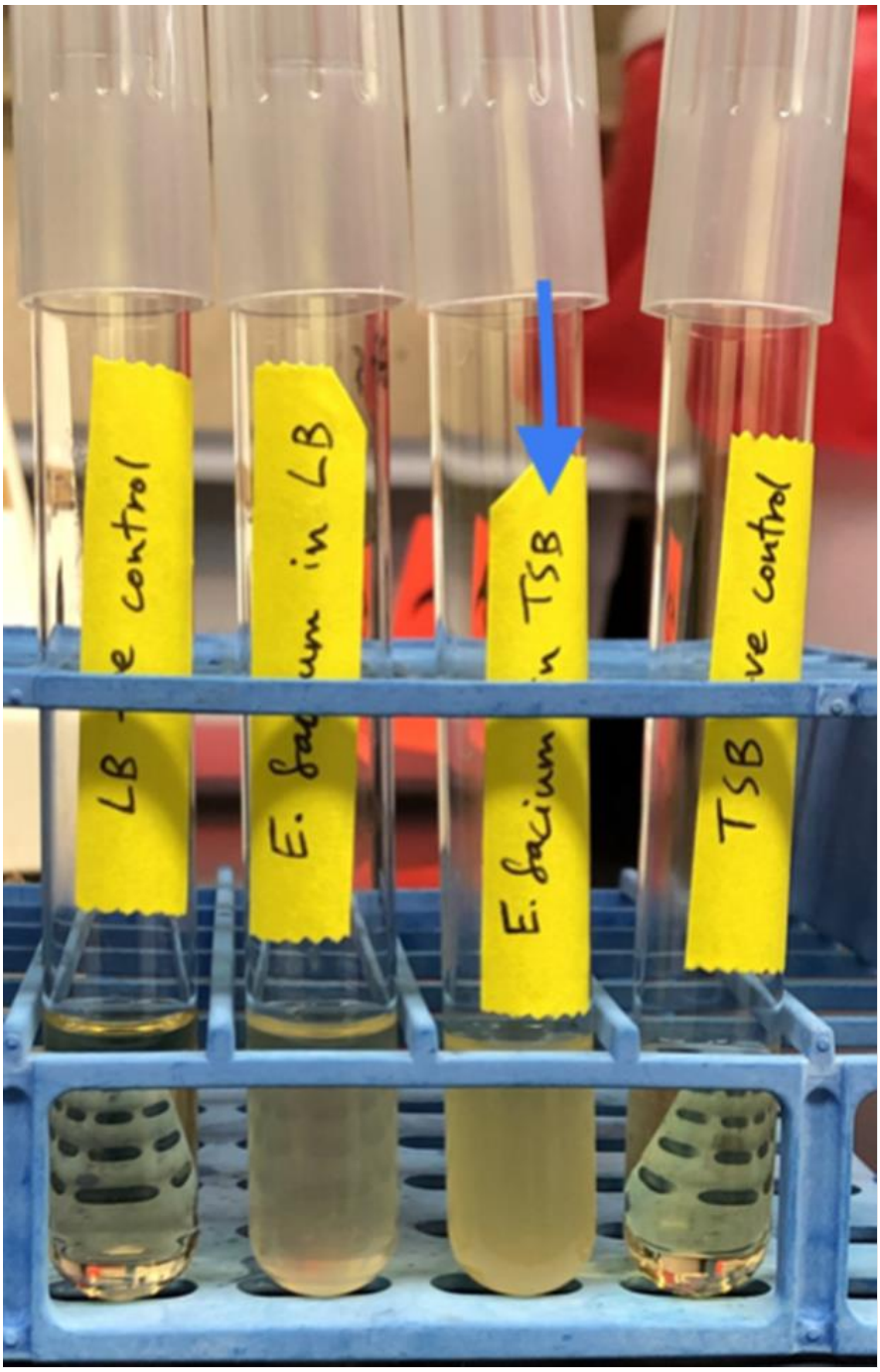

Figure 12: Comparison of *E. faecium* growth in LB and TSB. Tubes from the left to right contain LB negative control, *E, faecium* in LB, *E. faecium* in TSB, and TSB negative control.

However, since we harvested the bacterial cells through centrifugation and subsequently made a standardized concentration in PBS before performing our PDI investigations, we never

suspected that the antimicrobial PDI outcome would be impacted by the type of growth media used. On the contrary, the *E. faecium* when grown in TSB displayed higher PDI resistance than when it is grown in LB (Figure 13). Therefore, here we decided to use TSB to grow our organisms going forward and aimed to compare our LB PDI data versus TSB PDI data to understand if this would make a difference across both Gram-positive and Gram-negative organisms.

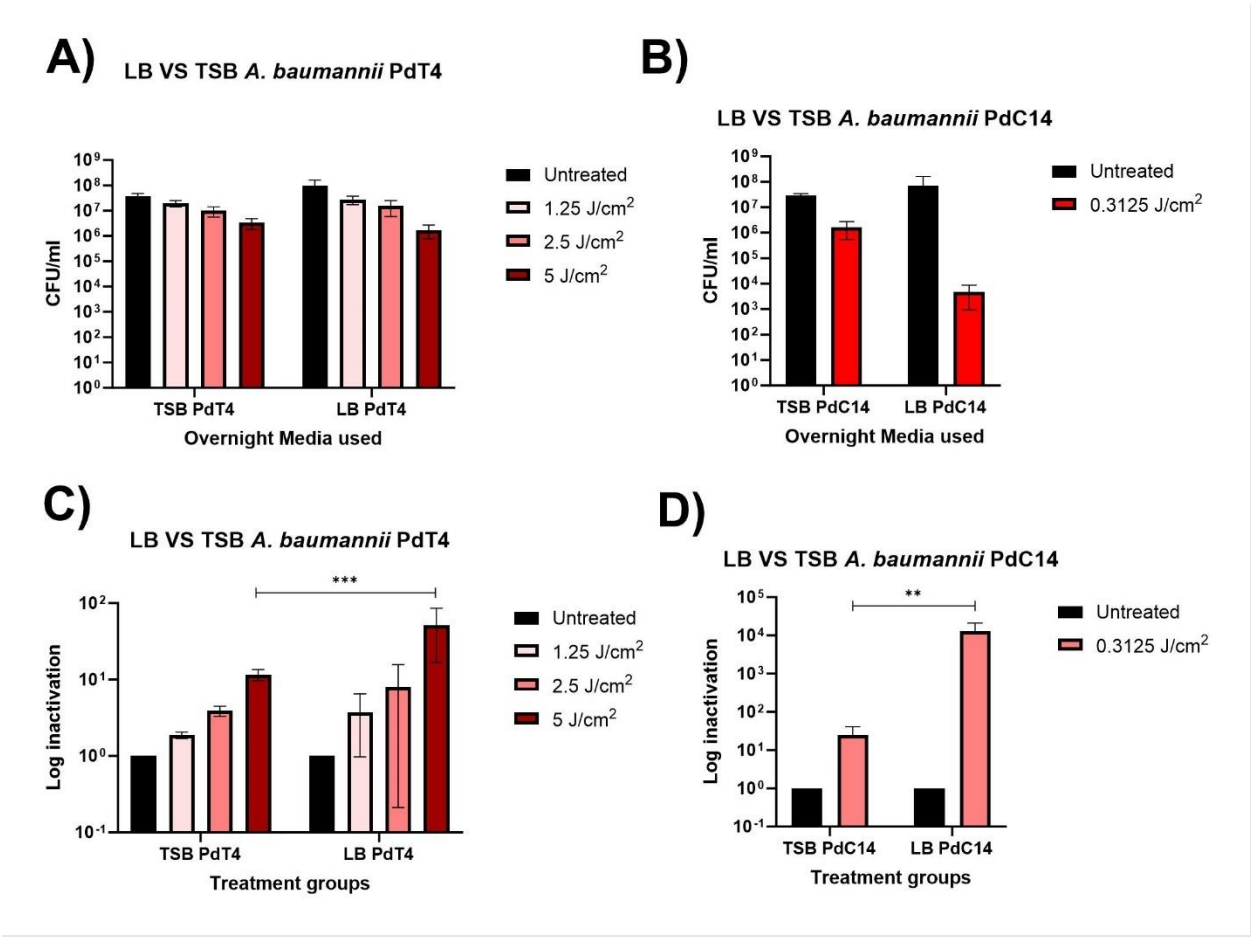

Figure 13: TSB VS LB PDI comparison against *A. baumannii*. PDI antimicrobial effect was compared in using TSB and LB as overnight growth media. Then, the harvested bacteria underwent similar treatments using 1 μM PdT4 and PdC14 concentrations. A) and B) PDI outcome expressed in CFU/ml. C) and D) PDI outcome expressed in log inactivation. Data represents at least 3-independent experiments with duplicate per experiment. ** $P \leq 0.005$, *** $P \leq 0.0005$.

In Gram-positive *E. faecium*, we initially noticed that the bacterium was extremely susceptible to PDI treatment using 1 μM PdT4 even at low irradiances when grown in LB. For example, at 0.15 J/cm^2 there was 3.61E+05 log inactivation, corresponding to 99.999% killing rate. However, when we ran the same PDI treatment using TSB we were unable to count the colonies due to overgrowth (Data not shown). This prompted us to switch our growth medium for *E. faecium* from LB to TSB to ensure a similar growth stage was achieved. Subsequently, the PDI results showed that at twice the irradiance 0.3125 J/cm^2, TSB grown *E. faecium* had 9.69E+01 log inactivation (97.82% killing rate) in three independent experiments (Figure 11B). It is important to note that we were unable to run statistical analysis here due to LB *E. faecium* PDI being less than 3-independent experiments.

In Gram-negative *A. baumannii*, there were no visual differences between overnight culture grown in both media (data not shown). Nonetheless, we needed to validate our LB obtained results, therefore, we reperformed our PDI experiments with 1 μM PdT4 using TSB instead. We analyzed the obtained 5 J/cm^2 irradiance log-inactivation data in LB-grown PdT4-treated *A. baumannii* (Figure 13C), 5.12E+01 log inactivation was achieved accounting for 98.78% killing rate, whereas 1.15E+01 log inactivation, corresponding to 90.97% killing rate, was achieved in TSB grown similarly treated *A. baumannii* (Figure 13C). In addition, two-way ANOVA analysis showed that there was a statistically significant difference ($P \leq 0.0005$) at the 5 J/cm^2 irradiance suggesting that changing the media does impact the outcome of PDI. When we switched to analyze the 1 μM PdC14 data, the results showed that LB grown *A. baumannii* was more sensitive to PDI treatment (Figure 13D). For example, at 0.3125 J/cm^2 irradiance, 1.30E+04 log inactivation (99.99% killing rate) was obtained over three independent experiments in LB whereas TSB grown *A. baumannii* showed higher survival rate with

2.48E+01 log inactivation (95.27% reduction in survival) using the same conditions (Figure 13B and 13D). Therefore, TSB grown *A. baumannii* shows a higher PDI treatment resistance when PdC14 is used as a PS and with PdT4 only at 5 J/cm^2 log inactivation. Statistical differences between LB and TSB treated *A. baumannii* were evident with PdC14 (Fig 13D; $P \leq 0.005$).

Overall, in both Gram-positive and Gram-negative bacterial pathogens, the selection of overnight culture growth media affects the outcome of PDI treatment. In conclusion, LB grown bacterial pathogens appear less resistant to PDI than TSB grown organisms. Based on our findings, we continued our PDI work using TSB as a general growth medium for our targeted organisms considering the growth stage would be more consistent between organisms.

II. Determining overall ESKAPE pathogens response to C14 PDI:

Next, we needed to understand if the Gram-positive and Gram-negative ESKAPE pathogens response to the C14 metalloporphyrin PDI would be different across their members. Therefore, we tested multiple members of the ESKAPE pathogens using PdC14 as well as ZnC14 (Figure 14).

A)

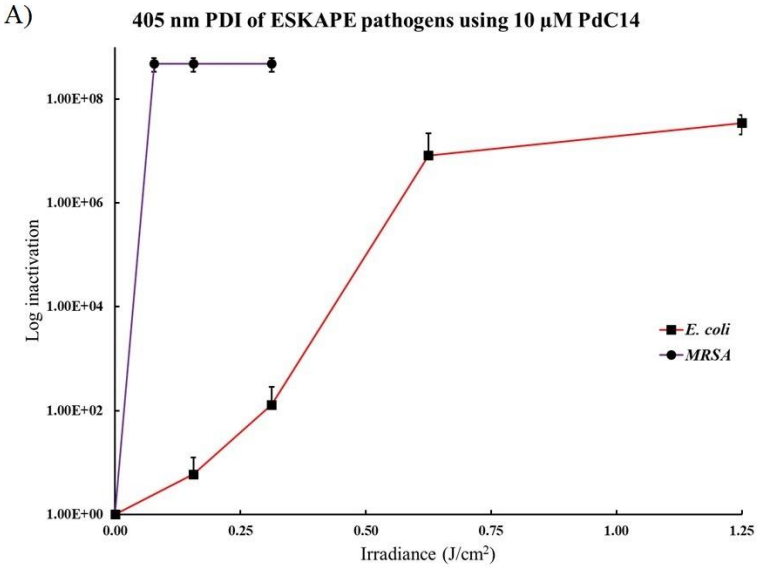
405 nm PDI of ESKAPE pathogens using 10 µM PdC14
Log inactivation
1.00E+08
1.00E+06
1.00E+04
1.00E+02
1.00E+00
0.00
0.25
0.50
0.75
1.00
1.25
Irradiance (J/cm²)
E. coli
MRSA

B)

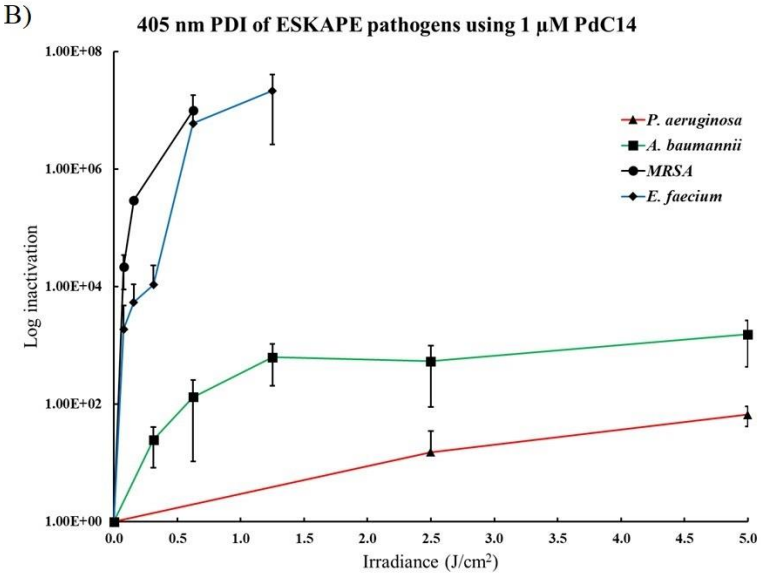
405 nm PDI of ESKAPE pathogens using 1 µM PdC14
Log inactivation
1.00E+08
1.00E+06
1.00E+04
1.00E+02
1.00E+00
0.0
0.5
1.0
1.5
2.0
2.5
3.0
3.5
4.0
4.5
5.0
Irradiance (J/cm²)
P. aeruginosa
A. baumannii
MRSA
E. faecium

C)

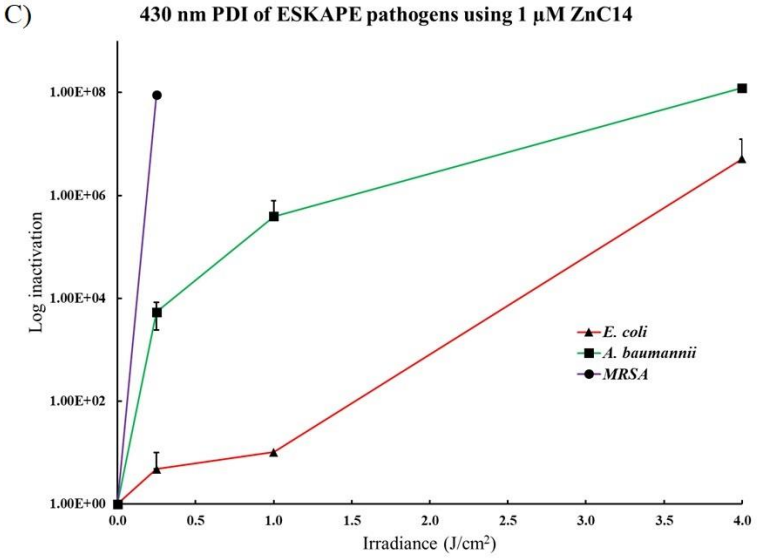
430 nm PDI of ESKAPE pathogens using 1 µM ZnC14
Log inactivation
1.00E+08
1.00E+06
1.00E+04
1.00E+02
1.00E+00
0.0
0.5
1.0
1.5
2.0
2.5
3.0
3.5
4.0
Irradiance (J/cm²)
E. coli
A. baumannii
MRSA

Figure 14: PDI using PdC14 and ZnC14 against ESKAPE pathogens. Organisms were incubated with corresponding metalloporphyrin 10 μM PdC14 (A), 1 μM PdC14 (B), and 1 μM ZnC14 (C) in the dark for 5 minutes. Then, exposed to 405 nm LED light in (A) and (B) or 430 nm LED light (C) at multiple irradiances. CFU/ml was determined by counting bacterial colonies the following day on TSA agar. LB was used for overnight cultures of (A) and (C) while TSB was used for (B). Purple lines represent Gram-positive organisms while red lines represent Gram-negative organisms. Data are representatives of 3 or less independent experiments with duplicates per experiment.

The results show that 10 μM PdC14 405 nm PDI was able to lyse *E. coli* (ATCC 11775) at 1.25 J/cm^2 (P<0.05) over three independent experiments whereas MRSA was fully inactivated at 0.039 J/cm^2 irradiance (P<0.05) (Figure 14A). Therefore, PdC14 is effective PS in PDI against both Gram-positive and Gram-negative ESKAPE pathogens. However, we never tested if the MRSA or *E. coli* using TSB as an overnight culture media at 10 μM PdC14 to see if the results would differ.

Then, we aimed to analyze the ESKAPE pathogens response to PdC14 PDI at 1 μM concentration (Figure 14B). We tested a total of four ESKAPE pathogens where two belong to Gram-positive, *E. faecium* and MRSA as well as two Gram-negative bacteria, *A. baumannii* and *P. aeruginosa* (Figure 14B). The results show that within the same group, different members of the ESKAPE pathogens display variation in their PDI response to PdC14 (Figure 14B). For example, MRSA was shown to be more sensitive to PDI treatment at 0.07 J/cm^2 irradiance with 2.19E+04 log inactivation, corresponding to 99.99% killing rate, whereas *E. faecium* showed a higher survival rate (99.67%) using the same irradiance with 1.91E+03 log inactivation in comparison (Figure 14 B, P-value < 0.05). Additionally, all MRSA bacteria were killed at 0.625 J/cm^2 irradiance whereas *E. faecium* showed 6.06E+06 log inactivation at the same irradiance corresponding to 99.999% killing rate (Figure 14B).

A similar trend was also observed with Gram-negative ESKAPE pathogens where *P. aeruginosa* shows higher resistance to 405 nm PDI relative to *A. baumannii* (Figure 14B). For example, at 2.5 J/cm^2, *A. baumannii* showed 5.43E+02 log inactivation, corresponding to 99.7% killing rate, whereby *P. aeruginosa* only showed 1.54E+01 log inactivation, accounting for 92.04% killing rate using the same treatment (Figure 14B). Also, at 5 J/cm^2, *A. baumannii* showed 1.55E+03 log inactivation, corresponding to 99.88% killing rate, whereas *P. aeruginosa* showed 6.72E+01 log inactivation in comparison accounting for 98.34% killing rate (*P*-value < 0.05) (Figure 14B). This is at least one log difference in survival rate between the two Gram-negative ESKAPE pathogens suggesting that individual members of the ESKAPE pathogens respond to PDI treatment differently.

Subsequently, we aimed to understand if the same story would occur with 1 μM ZnC14 (Figure 14C). Therefore, we tested MRSA, *A. baumannii*, and MDR *E. coli* (WDL-149) using 430 nm LED light (Figure 14C). As expected with Gram-positive PDI treatment, MRSA was sensitive to the PDI where it was entirely killed at 0.25 J/cm^2 (Figure 14C). However, the PDI response between *E. coli* versus *A. baumannii* shows that the latter is more sensitive to PDI using 1 μM ZnC14 (Figure 14C). For example, at 4 J/cm^2, *A. baumannii* was fully inactivated whereas *E. coli* showed an average of 5.15E+06 log inactivation accounting for 99.999% killing rate (Figure 14C).

In conclusion, C14 metalloporphyrin PDI works well against Gram-positive and Gram-negative ESKAPE pathogens. In addition, different members of the ESKAPE pathogens display different responses to PDI treatment with both PdC14 and ZnC14.

III. Determining if the PDI antimicrobial effect is binding dependent:

Having shown that the C14 metalloporphyrin has superior bacterial binding ability (Figures 3-8) and stronger PDI activity than the unsubstituted T4 (Figures 9-14), here we aimed to determine if the improved antimicrobial PDI outcome is attributable to bound porphyrin. Therefore, we incubated *E. faecium* with 1 μM PdT4 and with 1 μM PdC14 for five minutes in dark conditions. Then, we pelleted the bacterial cells, discarded the supernatant, washed the collected pellet twice with PBS, resuspended them, and subsequently, exposed the bacteria to 405 nm LED light to analyze the survival fraction relative to untreated as well as bound and unbound controls.

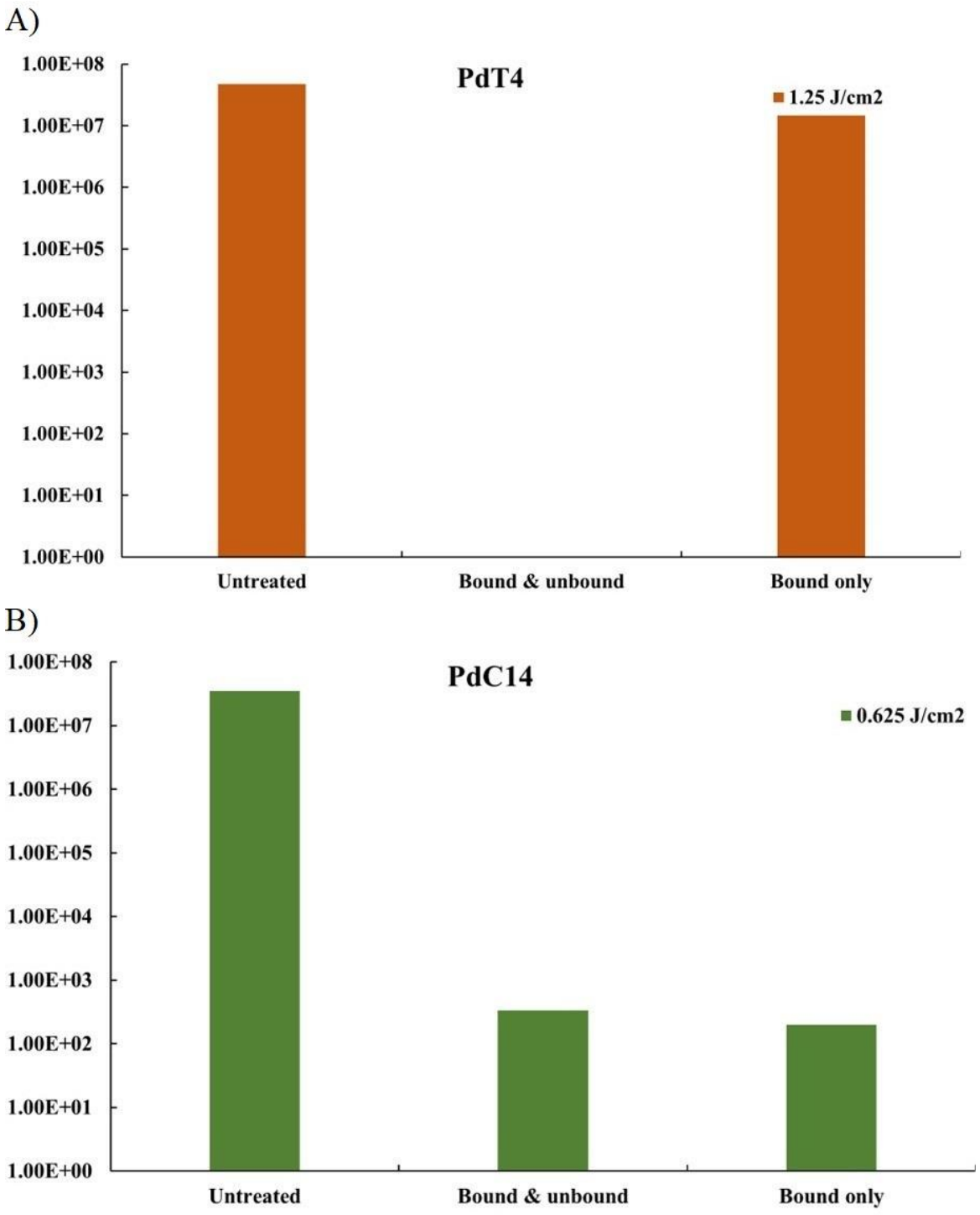

Figure 15: Binding dependence for antimicrobial PDI effect against *E. faecium*. PDI of *E. faecium* incubated with 1 μM PdT4 (A) and PdC14 (B). Bound & unbound: LED light exposure was carried out immediately after dark PS incubation. Bound only: the PS incubated cells were centrifuged and washed twice with PBS, then, exposed to LED light. Data are representative of single independent experiment with duplicates per experiment.

The results show that PDI eradicated *E. faecium* with PdT4 and 405 nm light independent of bound status (Figure 15A). However, for PdC14 PDI, there was a dependence on bound form (Figure 15B).

Although this is preliminary data with one experiment, these results are consistent with our previous findings in Specific aim 1 as well as Specific aim 2. In conclusion, PdC14 PDI antimicrobial activity relies on the PS binding towards the targeted organisms.

IV. Determining the bactericidal effect of ZnC14 against purified endospores:

Next, we were interested in evaluating the C14 metalloporphyrin PDI antimicrobial effect against a highly resistant form of bacteria. Therefore, we selected endospore-producing Gram-positive *B. cereus* as our organism of choice in this investigation. *B. cereus* was grown in sporulation media following published procedures (Banerjee et al., 2012; Demidova & Hamblin, 2005). Ultimately, we were able to drive the bacterium into its metabolically inactive sporulated state and purify them into 10 ml suspensions corresponding to 5.33E+07 CFU/ml (data not shown). Then, we proceeded to verify the purity of the collected endospores using malachite green staining (Figure 16), which shows over 99% of bacteria were stained endospores with the remaining being fragments of vegetative cells.

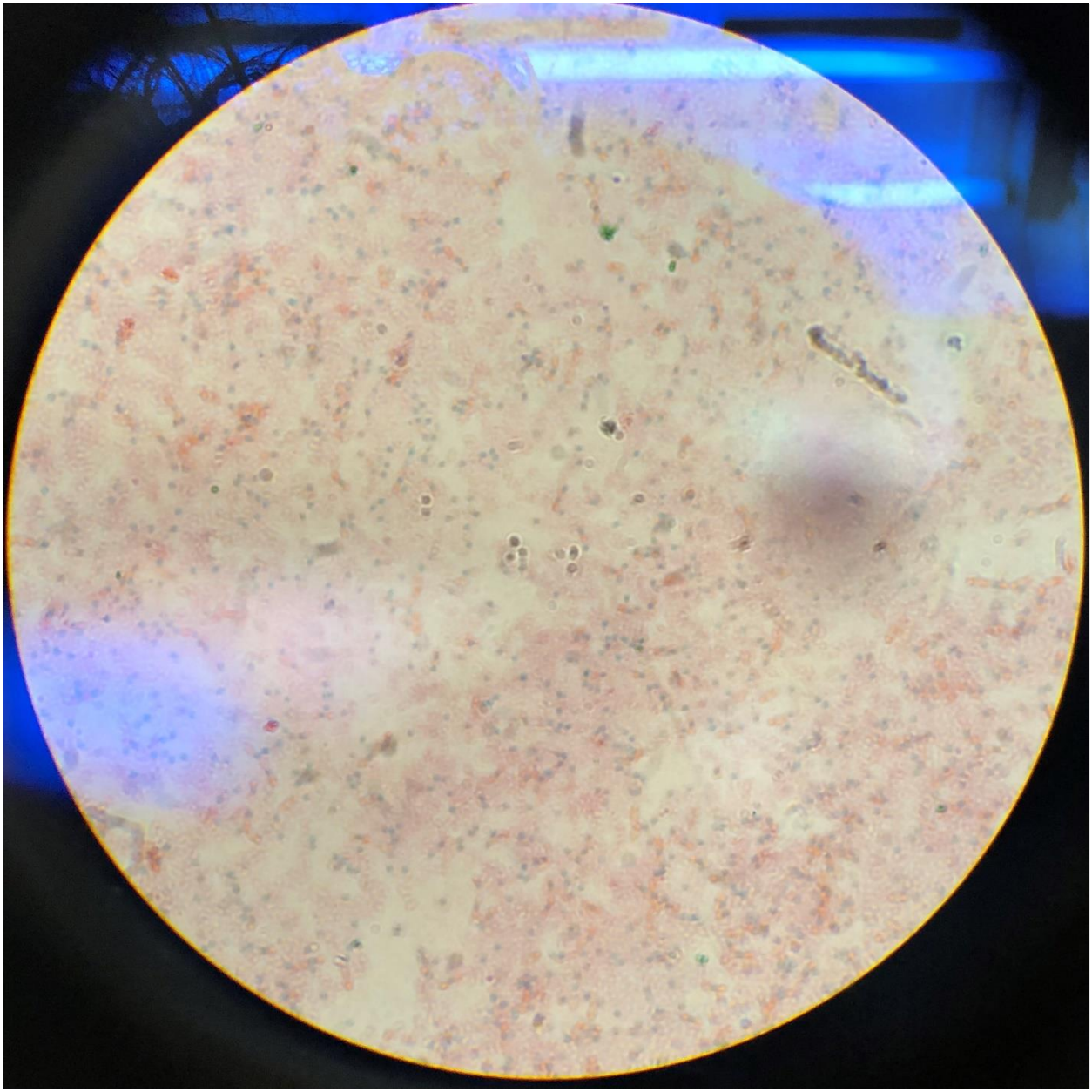

Figure 16: Purified *B. cereus* endospores stained with malachite green. Endospores are stained green while vegetative cell fragments were counter stained with safranin (pink). Picture was taken using light microspore with 1000x total magnification power.

Once we confirmed the endospores suspension concentration and purity, we initially tested their ability to withstand PDI treatment using 3 μM ZnC14 at 4.4 J/cm^2 irradiance (Figure 17A).

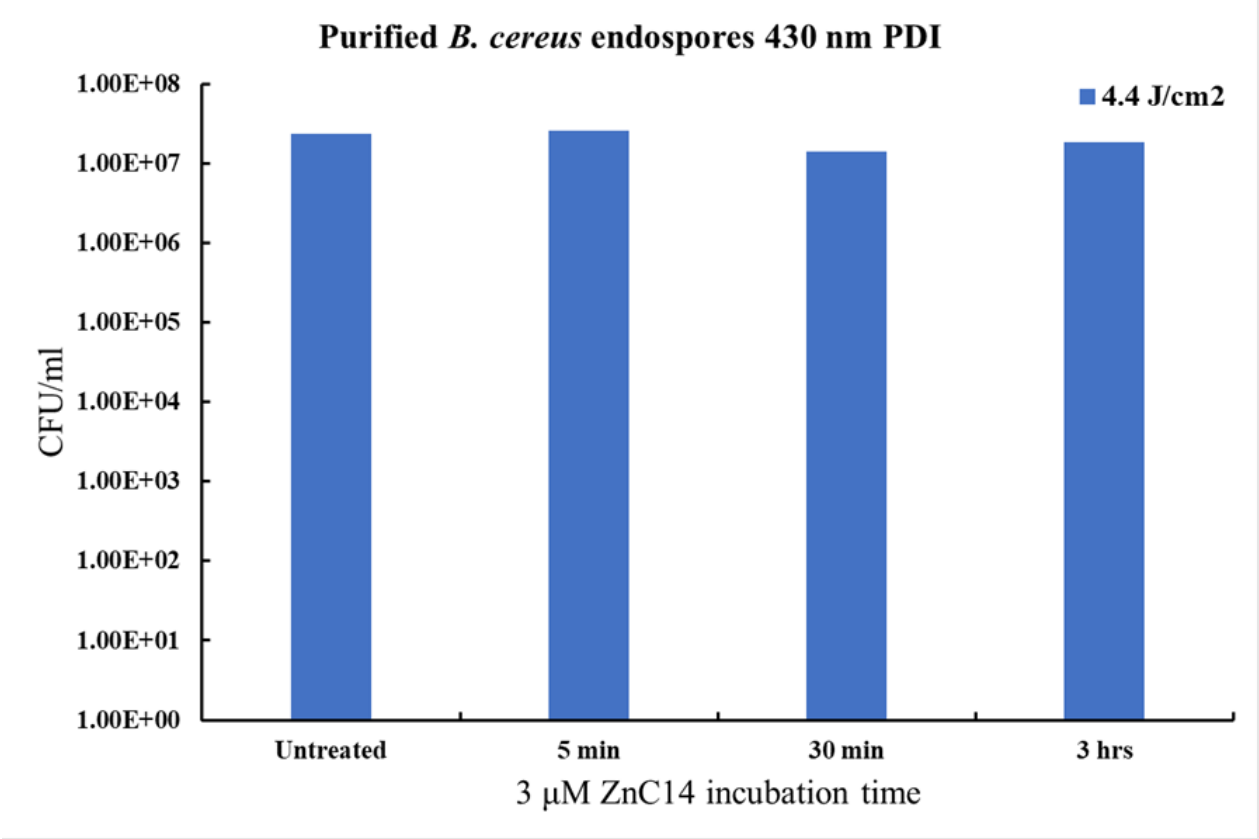

Figure 17: PDI of *B. cereus* purified endospores using ZnC14. The PDI tested endospores were incubated in dark condition using multiple time intervals with 3 μM ZnC14. Then the spores were exposed to 430 nm LED light at 4.4 J/cm^2. CFU/ml was determined through counting colonies on TSA plates. Each bar represents a single independent experiment with duplicates.

We divided our treatment groups into three different PS incubation times: 5, 30, and 180 minutes. PDI treatment results showed 2.57E+07, 1.40E+07, and 1.87E+07 CFU/ml in the 5 minutes, 30 minutes, and 180 minutes treatment groups respectively (Figure 17), compared to the original 2.37E+07 CFU/ml untreated group. These numbers correlate with -8.45%, 40.85%, and 21.13% killing rates. As a result, we realized that maybe a longer irradiation is needed before comparing incubation period.

As a result, we decided to drastically increase the ZnC14 concentration and the irradiance to analyze if that would make a difference against *B. cereus* purified endospores. Therefore, we

tested the purified spores using 20 μM ZnC14 incubation for 3 hours at 37˚ C before exposing to 90 J/cm^2 of 430 nm LED irradiance (data not shown). Unfortunately, however, The LED light device got damaged during the experiment. So, we never reached the 90 J/cm^2 we were aiming for, which corresponds to 30 minutes of light exposure. In addition, the negative control plates showed contamination of the 70% ethanol used and the spreader as well, rendering the results invalid. Nevertheless, we did notice a slight drop in the treated endospore suspension where the log inactivation was shown to be at least a 76% killing of endospores 4.20E+00 (data not shown). Considering the contamination would have resulted in more CFU in the treated group, we would hypothesize that if repeated the killing would be significantly higher.

In conclusion, these are merely preliminary data that suggests *B. cereus* endospores might be sensitive to killing via PDI treatment though more resistant than vegetative bacterial pathogens (Data not shown in *B. subtilis*).

CHAPTER 4: DISCUSSION

The purpose of this thesis was to investigate the PDI effects against ESKAPE pathogens using PS with increased lipophilicity via adding a C14 side chain, thus turning hydrophilic PdT4 and ZnT4 into amphiphilic PdC14 and ZnC14. We selected an array of ESKAPE pathogens and endospores antimicrobial PDI effect. Across both Gram-positive and Gram-negative, the addition of C14 improved PS bacterial bindings relative to unsubstituted metalloporphyrin. We also observed improved PDI antimicrobial effect associated with C14 addition. This was consistent in both Gram-positive and -negative ESKAPE pathogens. We also noticed that the C14 bactericidal activity heavily depended on bacterial binding unlike the T4 derivatives. We also noticed variation in PDI responses between TSB and LB grown bacteria using the same treatment. Preliminary data supported that C14 metalloporphyrin may work against more resilient forms of bacteria such as endospores and that the C14 metalloporphyrin bactericidal effects are dependent upon the bound portion of porphyrin.

Antimicrobial resistance has been shown to pose a clinical challenge, especially with ESKAPE pathogens (Li et al., 2021; Masoud et al., 2022; Mulani et al., 2019). Over the past decade, once a new antibiotic is discovered, microbial resistance occurs shortly thereafter (Browne et al., 2020). One of the alternative therapies to combat antimicrobial resistance is the use of bacteriophage. This approach allows the targeted bacteria to be infected with a virus that hijacks the cellular machinery ultimately leading to bacterial lysis thereby clearing human infections. However, this antibiotic alternative approach has its limitations as well. These limitations include the ability of the bacteria to undergo mutation where they become resistant to bacteriophage therapy (Hesse et al., 2020; Zulk et al., 2022). In PDI however, although

antioxidant enzymes such as catalase and SOD may provide some protection against ROS, the production of singlet oxygen has been shown to inactivate those enzymes (Kim et al., 2001). In addition, a 20 times passage study that aimed to investigate the ability of *P. aeruginosa*, *S. aureus*, and *Candida albicans* to develop resistance against PDI treatment concluded that there was no development of any resistant mutants (Giuliani et al., 2010). Therefore, PDI is an excellent alternative treatment to combat antimicrobial resistance.

Porphyrins are among the most studied PS in antimicrobial PDI (Alves et al., 2009; Banerjee et al., 2012; A. Oliveira et al., 2009; Sułek et al., 2020). The addition of C14 to TMPyP has been shown to increase its uptake by melanoma cells *in vitro* as well as *in vivo* (Rapozzi et al., 2014). Another study that evaluated the addition of alkyl chains to tetra-cationic TMPyP porphyrin ranging from C6-C22 which found that C10 and C14 substituted porphyrin analogues worked the best against MRSA and *E. coli* (Reddi et al., 2002). They also showed a 4.35 log reduction in *E. coli* cell survival using 1 μM C14 porphyrin analogue with white light irradiation at 135 J/cm^2 (Reddi et al., 2002). In comparison, our findings show an increased log inactivation (5.15E+06) of *E. coli* using the same concentration of metalloporphyrin with a fraction of the irradiance (4 J/cm^2) using 430 nm blue light (Figure 14C). It is also important to note that the C14 porphyrins used in our study differ in that we incorporated either Pd or Zn metal at their core structure. Nonetheless, these findings support that alkylation of porphyrins improves the antimicrobial PDI outcome.

The addition of metals such as Pd to porphyrin PS molecules has been shown to increase singlet oxygen yield due to intersystem crossing shifting the photochemical PDI reaction towards

Type-II, thereby improving overall phototoxicity (Hirohara et al., 2012; Obata et al., 2009). Compared to other metals, zinc derivatives have been shown to produce the most singlet oxygen (Mroz et al., 2009).We have shown before that the insertion of Zn and Pd to porphyrin results in a higher singlet oxygen production upon excitation with 405 nm LED light compared to T4 as well as other metalloporphyrins (Skwor et al., 2016). One publication that investigated the antimicrobial PDI activity of C12 metalloporphyrin, with and without Pd, concluded that the insertion of Pd metal to C12 porphyrin improves antimicrobial PDI activity (Xuan et al., 2019). They showed that over 6 logs MRSA reduction was achieved using 0.01 μM PdC12 with 415 nm blue light at 10 J/cm^2 irradiance (Xuan et al., 2019). In our research, we were able to achieve over 4 logs inactivation of MRSA using a much lower irradiance (0.05 J/cm^2) though at a slightly higher PS concentration (0.1 μM ZnC14) (Data not shown), as well as over 7-log inactivation at 0.25 J/cm^2 using 1 μM ZnC14 (Figure 14C). While they found that *E. coli* showed PdC12 PDI was able to achieve over 2 logs reduction at 5 J/cm^2 (Xuan et al., 2019), we have been able to show over 3 logs inactivation of *A. baumannii* with PdC14 using the same irradiance, but with higher PdC14 concentration (1 μM PdC14) (Figure 11D). In conclusion, our findings agree with other publications.

One of our findings during this study is that the selection of overnight growth media may influence the outcome of PDI experiments. For example, we have observed that LB grown organisms displayed a higher sensitivity towards PDI compared to the same TSB grown organisms (Figure 12). Specifically, *A. baumannii* showed more resistance to PdC14 PDI treatment when grown in TSB as opposed to LB (Figure 13). These findings were unexpected because both media were utilized with the aim of growing our targeted bacteria to allow cellular

harvesting for downstream experiments. For instance, regardless of the growth in quantity, enough cells were collected through centrifugation to make a standardized bacterial suspension in PBS for PDI experiments. Yet, the PDI outcome changed for the same organisms between the two media in spite of standardizing the bacterial suspension concentration. Generally, the life cycle of microorganisms in growth media go through four phases: the lag phase, the exponential phase, the stationary phase, and lastly the death phase (Navarro Llorens et al., 2010). The lag phase represents a brief delay before the start of replication process, the exponential phase is where the bacterial cells undergo cellular division at a constant rate, the stationary phase is where the bacteria stop replicating due to growth unfavorable conditions, and finally the death phase is when the bacterial cells lose viability (Navarro Llorens et al., 2010). If the stationary phase is reached by the time the bacterial cells are collected from media, this may affect the PDI vulnerability. For example, it has been shown that *S. aureus* and *S. epidermidis* were more susceptible to PDI treatment due to higher PS uptake during exponential phase than during stationary phase (Gad et al., 2004). Therefore, different growth media can cause variations in antimicrobial PDI response depending on how fast stationary phase is reached. Despite the wide use of LB in research due to its ability to support the growth of many organisms, one of its limitations is that of the source of utilizable carbons. While TSB contains casein peptone, soy peptone, K_2HPO_4, NaCl, and glucose as a carbohydrate source, LB does not contain carbohydrates, but contains 10 g peptone, 5 g yeast extract, and 0.5 g NaCl per liter instead. One study showed that *E. coli* exponential phase growth ceases at 0.3 OD600 value followed by slow growth rate and decrease in *E. coli* average cell size (Sezonov et al., 2007). Once *E. coli* ceased to further grow in LB, the medium was collected through centrifugation and re-inoculated with the same organism with no growth observed (Sezonov et al., 2007). However, upon glucose

addition to the nutrient depleted LB, *E. coli* grew once re-inoculated (Sezonov et al., 2007). Therefore, it is possible that the lack of carbohydrates within this medium may negatively affect bacterial growth rendering increased PDI susceptibility as seen in our findings (Figures 12 and 13). Although it has been characterized in *S. aureus* biofilm PDI (Reynoso et al., 2019), to the best of my knowledge, there are no PDI studies in the literature that analyze the effect of using multiple growth media for the same organism on the PDI antimicrobial outcome, which highlights a possible gap in knowledge within the PDI field of study. In conclusion, based on our findings (Figures 12 and 13), we do not recommend using LB as growth media for PDI studies.

In terms of bacterial binding, our findings agree with another study that found that the alkylation of tetra-cationic TMPyP PS improves bacterial binding (Reddi et al., 2002). For example, C10, C14, and C22 TMPyP substitutions demonstrated an increased detection of the PS in *S. aureus* and *E. coli* relative to the unsubstituted derivative (Reddi et al., 2002). Similarly, our binding results show increased PS uptake in C14 metalloporphyrin derivatives compared to T4 metalloporphyrin derivatives in MRSA, *E. faecium*, and *A. baumannii* (Figures 3-8). Our PS derivatives are unique in the sense that they contain metals, Pd or Zn, at the center of the porphyrin, but similar bacterial binding observations were made in *E. faecium* and *A. baumannii*.

PDI against *Bacillus* endospores has been shown to work against purified endospores (Banerjee et al., 2012; Demidova & Hamblin, 2005; A. Oliveira et al., 2009). The caveate however, is that PDI against endospores requires a high PS concentration as well as high irradiance. Furthermore, it has been shown that no more than 3-log inactivation at 1690 W/m^2 for two minutes of white light exposure using 60 μM methyl tetra-cationic porphyrin can be achieved in spite of higher PS concentration and higher irradiance (A. Oliveira et al., 2009). In

our line of experiments, we aimed to understand if the newly developed ZnC14 would work against sporulated *B. cereus*. It has been established already that PdT4 did not affect purified *B. subtilis* endospores using 405 nm LED light (data not shown). Therefore, we decided to select *B. cereus* endospores because it has been shown that it responds better to PDI treatments (Demidova & Hamblin, 2005). The variations within the spore coating structure composition in terms of the crust, inner coat, and outer coat could make *Bacillus* species respond differently to PDI treatment (Driks & Eichenberger, 2016). In the context of our experiments, we were unable to find remarkable differences across multiple ZnC14 pre-incubation periods (Figure 17). Nevertheless, both *B. cereus* endospores PDI experiments we performed provided preliminary data regarding optimizing the ZnC14 PDI treatment. Overall, the ZnC14 with 430 nm LED PDI may still work against *B. cereus* endospores. However, that would probably require higher PS concentration as well as higher irradiance dosages.

CHAPTER 5: CONCLUSIONS AND FUTURE DIRECTIONS

Future studies involving murine model are warranted to further understand the impact of PDI treatment on clincial infections, most likely wound infections. Other studies have supported the use of PDI against wound infections in animal models using similar TMPyP derivatives, as well as other PS such as phenothiazinium-based derivatives (Xiao et al., 2021; Xu et al., 2016). However, the impact of adding C14 side chain to Pd- and Zn-metalloporphyrin on murine wound infections should be further characterized considering similar PS have worked *in vivo*. Another disease that might benefit from PDI studies is *Chlamydia trachomatis* infections. We are not aware of any PDI studies assessing its applicability against this intracellular pathogen, although phototherapy with blue light has shown some bactericidal effects (Wasson et al., 2012). During our experiments, we tried testing if *Chlamydia trachomatis* serovar E would be prone to PDI treatment. However, our frozen *Chlamydia* stock did not appear viable for the few experiments performed. *Chlamydia* PDI research remains unexplored though its impact on the metabolically inactive *Chlamydia* elementary body would be of strong interest to the scientific community.

In conclusion, we have been able to show in our studies that the addition of C14 side chain to PdT4 and ZnT4, improves the ability of the two PS to bind to both Gram-positive and Gram-negative ESKAPE pathogens. Additionally, it improves the overall PDI antimicrobial efficiency using blue LED light. Furthermore, we showed preliminary data highlighting that the C14 substituted metalloporphyrin relies on binding to exert their antimicrobial PDI outcome, as well as its potential against purified *B. cereus* endospores. We have also highlighted that C-1 associated antimicrobial activity improves regardless of Zn or Pd metal insertion into the PS.

Finally, we have shown that the selection of overnight growth media may greatly impact the bacterial response to PDI treatment.

REFERENCES:

Albarracin, R., Eells, J., & Valter, K. (2011). Photobiomodulation protects the retina from light-induced photoreceptor degeneration. *Investigative Ophthalmology & Visual Science*, *52*(6), 3582–3592. https://doi.org/10.1167/IOVS.10-6664

Alves, E., Costa, L., Carvalho, C. M., Tomé, J. P., Faustino, M. A., Neves, M. G., Tomé, A. C., Cavaleiro, J. A., Cunh, A., & Almeida, A. (2009). Charge effect on the photoinactivation of Gram-negative and Gram-positive bacteria by cationic meso-substituted porphyrins. *BMC Microbiology*, *9*. https://doi.org/10.1186/1471-2180-9-70

Amara, S., Adamson, R. T., Lew, I., & Huang, X. (2013). Clinical response at Day 3 of therapy and economic outcomes in hospitalized patients with acute bacterial skin and skin structure infection (ABSSSI). *Current Medical Research and Opinion*, *29*(7), 869–877. https://doi.org/10.1185/03007995.2013.803056

American Academy of Pediatrics. (2019, November 15). *The History of Antibiotics - HealthyChildren.org*. https://www.healthychildren.org/English/health-issues/conditions/treatments/Pages/The-History-of-Antibiotics.aspx

Banerjee, I., Mehta, K. K., Dordick, J. S., & Kane, R. S. (2012). Light-activated porphyrin-based formulations to inactivate bacterial spores. *Journal of Applied Microbiology*, *113*(6), 1461–1467. https://doi.org/10.1111/J.1365-2672.2012.05438.X

Bartoszewicz, M., & Czyżewska, U. (2021). Comparison of the antibiotic resistance between genetically diverse and toxigenic Bacillus cereus sensu lato from milk, pepper and natural habitats. *Journal of Applied Microbiology*, *130*(2), 370–381. https://doi.org/10.1111/JAM.14792

Browne, K., Chakraborty, S., Chen, R., Willcox, M. D. P., Black, D. S., Walsh, W. R., & Kumar, N. (2020). A New Era of Antibiotics: The Clinical Potential of Antimicrobial Peptides. *International Journal of Molecular Sciences*, *21*(19), 1–23. https://doi.org/10.3390/IJMS21197047

Castano, A. P., Demidova, T. N., & Hamblin, M. R. (2004). Mechanisms in photodynamic therapy: part one-photosensitizers, photochemistry and cellular localization. *Photodiagnosis and Photodynamic Therapy*, *1*(4), 279–293. https://doi.org/10.1016/S1572-1000(05)00007-4

Centers for Disease Control and Prevention (CDC). (2019). *Antibiotic Resistance Threats in the United States, 2019*. https://doi.org/10.15620/cdc:82532

Centers for Disease Control and Prevention (CDC). (2022, October 5). *About Antibiotic Resistance | CDC*. https://www.cdc.gov/drugresistance/about.html

Chandra, S., Qureshi, S., Chopra, D., Dwivedi, A., & Ray, R. S. (2022). Involvement of Type-I and Type-II Photodynamic Reactions in Photosensitization of Fragrance Ingredient 2-acetonaphthone. *Photochemistry and Photobiology*, *98*(5), 1050–1058. https://doi.org/10.1111/PHP.13593

De Oliveira, D. M. P., Forde, B. M., Kidd, T. J., Harris, P. N. A., Schembri, M. A., Beatson, S. A., Paterson, D. L., & Walker, M. J. (2020). Antimicrobial Resistance in ESKAPE Pathogens. *Clinical Microbiology Reviews*, *33*(3). https://doi.org/10.1128/CMR.00181-19

de Vasconcelos Catão, M. H. C., Nonaka, C. F. W., de Albuquerque, R. L. C., Bento, P. M., & de Oliveira Costa, R. (2015). Effects of red laser, infrared, photodynamic therapy, and green LED on the healing process of third-degree burns: clinical and histological study in rats. *Lasers in Medical Science*, *30*(1), 421–428. https://doi.org/10.1007/S10103-014-1687-0

Demidova, T. N., & Hamblin, M. R. (2005). Photodynamic inactivation of Bacillus spores, mediated by phenothiazinium dyes. *Applied and Environmental Microbiology*, *71*(11), 6918–6925. https://doi.org/10.1128/AEM.71.11.6918-6925.2005

do Amparo Manoel, C., de Sousa Mariano, S., da Silva Ramos, E., Paolillo, F. R., de Aro, A. A., Mendes, C., Venturini, L. M., Silveira, P. C. L., Bagnato, V. S., & de Andrade, T. A. M. (2022). Photobiomodulation and photodynamic therapy applied after electrocauterization for skin healing optimization in rats. *Journal of Biophotonics*, *15*(5). https://doi.org/10.1002/JBIO.202100239

Driks, A., & Eichenberger, P. (2016). The Spore Coat. *Microbiology Spectrum*, *4*(2). https://doi.org/10.1128/MICROBIOLSPEC.TBS-0023-2016/ASSET/CBA87C29-3A68-4E9E-8639-B4EA5E941E7E/ASSETS/GRAPHIC/TBS-0023-2016-FIG3.GIF

Dull, P. M., Wilson, K. E., Kournikakis, B., Whitney, E. A. S., Boulet, C. A., Ho, J. Y. W., Ogston, J., Spence, M. R., Mckenzie, M. M., Phelan, M. A., Popovic, T., & Ashford, D. (2002). Bacillus anthracis Aerosolization Associated with a Contaminated Mail Sorting Machine - Volume 8, Number 10—October 2002 - Emerging Infectious Diseases journal - CDC. *Emerging Infectious Diseases*, *8*(10), 1044–1047. https://doi.org/10.3201/EID0810.020356

Eichner, A., Gonzales, F. P., Felgenträger, A., Regensburger, J., Holzmann, T., Schneider-Brachert, W., Bäumler, W., & Maisch, T. (2013). Dirty hands: photodynamic killing of human pathogens like EHEC, MRSA and Candida within seconds. *Photochemical & Photobiological Sciences : Official Journal of the European Photochemistry Association and the European Society for Photobiology*, *12*(1), 135–147. https://doi.org/10.1039/C2PP25164G

Fakhry, S. M., MacLeod, K., Shen, Y., Garland, J. M., Wyse, R. J., McLean, L., Wilson, N. Y., Morse, J. L., & Watts, D. D. (2022). Bacteremia in Trauma: A Contemporary Analysis of Blood Culture Results and Outcomes in 158,884 Patients. *Surgical Infections*, *23*(9), 809–816. https://doi.org/10.1089/SUR.2022.228

Ferrer-Espada, R., Liu, X., Goh, X. S., & Dai, T. (2019). Antimicrobial Blue Light Inactivation of Polymicrobial Biofilms. *Frontiers in Microbiology*, *10*(APR). https://doi.org/10.3389/FMICB.2019.00721

Fleming, I. D., Krezalek, M. A., Belogortseva, N., Zaborin, A., Defazio, J., Chandrasekar, L., Actis, L. A., Zaborina, O., & Alverdy, J. C. (2017). Modeling Acinetobacter baumannii wound infections: The critical role of iron. *The Journal of Trauma and Acute Care Surgery*, *82*(3), 557–565. https://doi.org/10.1097/TA.0000000000001338

Gad, F., Zahra, T., Hasan, T., & Hamblin, M. R. (2004). Effects of growth phase and extracellular slime on photodynamic inactivation of gram-positive pathogenic bacteria. *Antimicrobial Agents and Chemotherapy*, *48*(6), 2173–2178. https://doi.org/10.1128/AAC.48.6.2173-2178.2004

Gamelas, S. R. D., Vieira, C., Bartolomeu, M., Faustino, M. A. F., Tomé, J. P. C., Tomé, A. C., Almeida, A., & Lourenço, L. M. O. (2022). Photodynamic inactivation of pathogenic Gram-negative and Gram-positive bacteria mediated by Si(IV) phthalocyanines bearing axial ammonium units. *Journal of Photochemistry and Photobiology. B, Biology*, *233*. https://doi.org/10.1016/J.JPHOTOBIOL.2022.112502

Gao, P., Munir, M., & Xagoraraki, I. (2012). Correlation of tetracycline and sulfonamide antibiotics with corresponding resistance genes and resistant bacteria in a conventional municipal wastewater treatment plant. *Science of The Total Environment*, *421–422*, 173–183. https://doi.org/10.1016/J.SCITOTENV.2012.01.061

Garcez, A. S., Núñez, S. C., Azambuja, N., Fregnani, E. R., Rodriguez, H. M. H., Hamblin, M. R., Suzuki, H., & Ribeiro, M. S. (2013). Effects of photodynamic therapy on Gram-positive and Gram-negative bacterial biofilms by bioluminescence imaging and scanning electron microscopic analysis. *Photomedicine and Laser Surgery*, *31*(11), 519–525. https://doi.org/10.1089/PHO.2012.3341

Giddins, M. J., Macesic, N., Annavajhala, M. K., Stump, S., Khan, S., McConville, T. H., Mehta, M., Gomez-Simmonds, A., & Uhlemanna, A. C. (2018). Successive Emergence of Ceftazidime-Avibactam Resistance through Distinct Genomic Adaptations in blaKPC-2-Harboring Klebsiella pneumoniae Sequence Type 307 Isolates. *Antimicrobial Agents and Chemotherapy*, *62*(3). https://doi.org/10.1128/AAC.02101-17

Giuliani, F., Martinelli, M., Cocchi, A., Arbia, D., Fantetti, L., & Roncucci, G. (2010). In Vitro Resistance Selection Studies of RLP068/Cl, a New Zn(II) Phthalocyanine Suitable for Antimicrobial Photodynamic Therapy. *Antimicrobial Agents and Chemotherapy*, *54*(2), 637. https://doi.org/10.1128/AAC.00603-09

Hamouda, T., Shih, A. Y., & Baker, J. R. (2002). A rapid staining technique for the detection of the initiation of germination of bacterial spores. *Letters in Applied Microbiology*, *34*(2), 86–90. https://doi.org/10.1046/J.1472-765X.2002.01047.X

Heffron, J., Bork, M., Mayer, B. K., & Skwor, T. (2021). A Comparison of Porphyrin Photosensitizers in Photodynamic Inactivation of RNA and DNA Bacteriophages. *Viruses*, *13*(3). https://doi.org/10.3390/V13030530

Heitkamp, R. A., Li, P., Mende, K., Demons, S. T., Tribble, D. R., & Tyner, S. D. (2018). Association of Enterococcus spp. with Severe Combat Extremity Injury, Intensive Care, and Polymicrobial Wound Infection. *Surgical Infections*, *19*(1), 95–103. https://doi.org/10.1089/SUR.2017.157

Herc, E. S., Kauffman, C. A., Marini, B. L., Perissinotti, A. J., & Miceli, M. H. (2017). Daptomycin nonsusceptible vancomycin resistant Enterococcus bloodstream infections in patients with hematological malignancies: risk factors and outcomes. *Leukemia & Lymphoma*, *58*(12), 2852–2858. https://doi.org/10.1080/10428194.2017.1312665

Hesse, S., Rajaure, M., Wall, E., Johnson, J., Bliskovsky, V., Gottesman, S., & Adhya, S. (2020). Phage Resistance in Multidrug-Resistant Klebsiella pneumoniae ST258 Evolves via Diverse Mutations That Culminate in Impaired Adsorption. *MBio*, *11*(1). https://doi.org/10.1128/MBIO.02530-19

Hirohara, S., Kawasaki, Y., Funasako, R., Yasui, N., Totani, M., Alitomo, H., Yuasa, J., Kawai, T., Oka, C., Kawaichi, M., Obata, M., & Tanihara, M. (2012). Sugar and heavy atom effects of glycoconjugated chlorin palladium complex on photocytotoxicity. *Bioconjugate Chemistry*, *23*(9), 1881–1890. https://doi.org/10.1021/BC300223J

Hsu, J. T., Chen, Y. W., Ho, T. W., Tai, H. C., Wu, J. M., Sun, H. Y., Hung, C. S., Zeng, Y. C., Kuo, S. Y., & Lai, F. (2019). Chronic wound assessment and infection detection method. *BMC Medical Informatics and Decision Making*, *19*(1). https://doi.org/10.1186/S12911-019-0813-0

Huang, L., Xuan, Y., Koide, Y., Zhiyentayev, T., Tanaka, M., & Hamblin, M. R. (2012). Type I and Type II mechanisms of antimicrobial photodynamic therapy: an in vitro study on gram-negative and gram-positive bacteria. *Lasers in Surgery and Medicine*, *44*(6), 490–499. https://doi.org/10.1002/LSM.22045

Iguchi, S., Mizutani, T., Hiramatsu, K., & Kikuchi, K. (2016). Rapid Acquisition of Linezolid Resistance in Methicillin-Resistant Staphylococcus aureus: Role of Hypermutation and Homologous Recombination. *PloS One*, *11*(5). https://doi.org/10.1371/JOURNAL.PONE.0155512

Jutkina, J., Rutgersson, C., Flach, C. F., & Joakim Larsson, D. G. (2016). An assay for determining minimal concentrations of antibiotics that drive horizontal transfer of resistance. *The Science of the Total Environment*, *548–549*, 131–138. https://doi.org/10.1016/J.SCITOTENV.2016.01.044

Kim, S. Y., Kwon, O. J., & Park, J. W. (2001). Inactivation of catalase and superoxide dismutase by singlet oxygen derived from photoactivated dye. *Biochimie*, *83*(5), 437–444. https://doi.org/10.1016/S0300-9084(01)01258-5

Kimáková, P., Solár, P., Fecková, B., Sačková, V., Solárová, Z., Ilkovičová, L., & Kello, M. (2017). Photoactivated hypericin increases the expression of SOD-2 and makes MCF-7 cells resistant to photodynamic therapy. *Biomedicine & Pharmacotherapy = Biomedecine & Pharmacotherapie*, *85*, 749–755. https://doi.org/10.1016/J.BIOPHA.2016.11.093

Klevens, R. M., Morrison, M. A., Nadle, J., Petit, S., Gershman, K., Ray, S., Harrison, L. H., Lynfield, R., Dumyati, G., Townes, J. M., Craig, A. S., Zell, E. R., Fosheim, G. E., McDougal, L. K., Carey, R. B., & Fridkin, S. K. (2007). Invasive methicillin-resistant Staphylococcus aureus infections in the United States. *JAMA*, *298*(15), 1763–1771. https://doi.org/10.1001/JAMA.298.15.1763

Kondo, K., Kawano, M., & Sugai, M. (2021). Distribution of Antimicrobial Resistance and Virulence Genes within the Prophage-Associated Regions in Nosocomial Pathogens. *MSphere*, *6*(4). https://doi.org/10.1128/MSPHERE.00452-21

Kubota, N., Kobayashi, J., Kasai, A., Nasuno, M., Murai, T., Minami, K., & Ohta, M. (2022). Detection of Bacillus cereus as a causative agent of emetic food poisoning by an unconventional culture procedure. *Journal of Infection and Chemotherapy : Official Journal of the Japan Society of Chemotherapy*, *28*(11), 1575–1577. https://doi.org/10.1016/J.JIAC.2022.07.011

Li, Z., Xie, J., Yang, J., Liu, S., Ding, Z., Hao, J., Ding, Y., Zeng, Z., & Liu, J. (2021). Pathogenic Characteristics and Risk Factors for ESKAPE Pathogens Infection in Burn Patients. *Infection and Drug Resistance*, *14*, 4727–4738. https://doi.org/10.2147/IDR.S338627

Lu, M., Dai, T. H., Hu, S. S., Zhang, Q., Bhayana, B., Wang, L., & Wu, M. X. (2020). Antimicrobial blue light for decontamination of platelets during storage. *Journal of Biophotonics*, *13*(1). https://doi.org/10.1002/JBIO.201960021

Mao, D., Yu, S., Rysz, M., Luo, Y., Yang, F., Li, F., Hou, J., Mu, Q., & Alvarez, P. J. J. (2015). Prevalence and proliferation of antibiotic resistance genes in two municipal wastewater treatment plants. *Water Research*, *85*, 458–466. https://doi.org/10.1016/J.WATRES.2015.09.010

Marturano, J. E., Ave, H., Marturano, J. E., & Lowery, T. J. (2019). ESKAPE Pathogens in Bloodstream Infections Are Associated With Higher Cost and Mortality but Can Be Predicted Using Diagnoses Upon Admission. *Open Forum Infectious Diseases*, *6*(12). https://doi.org/10.1093/OFID/OFZ503

Masoud, S. S., Kovacevich, A., Gangji, R., Nyawale, H., Nyange, M., & Ntukula, A. (2022). Extent and Resistance Patterns of ESKAPE Pathogens Isolated in Pus Swabs from

Hospitalized Patients. *The Canadian Journal of Infectious Diseases & Medical Microbiology = Journal Canadien Des Maladies Infectieuses et de La Microbiologie Medicale*, *2022*. https://doi.org/10.1155/2022/3511306

Mroz, P., Bhaumik, J., Dogutan, D. K., Aly, Z., Kamal, Z., Khalid, L., Kee, H. L., Bocian, D. F., Holten, D., Lindsey, J. S., & Hamblin, M. R. (2009). Imidazole metalloporphyrins as photosensitizers for photodynamic therapy: role of molecular charge, central metal and hydroxyl radical production. *Cancer Letters*, *282*(1), 63–76. https://doi.org/10.1016/J.CANLET.2009.02.054

Muehler, D., Brandl, E., Hiller, K. A., Cieplik, F., & Maisch, T. (2022). Membrane damage as mechanism of photodynamic inactivation using Methylene blue and TMPyP in Escherichia coli and Staphylococcus aureus. *Photochemical & Photobiological Sciences : Official Journal of the European Photochemistry Association and the European Society for Photobiology*, *21*(2), 209–220. https://doi.org/10.1007/S43630-021-00158-Z

Mulani, M. S., Kamble, E. E., Kumkar, S. N., Tawre, M. S., & Pardesi, K. R. (2019). Emerging Strategies to Combat ESKAPE Pathogens in the Era of Antimicrobial Resistance: A Review. *Frontiers in Microbiology*, *10*(APR), 539. https://doi.org/10.3389/FMICB.2019.00539

Navarro Llorens, J. M., Tormo, A., & Martínez-García, E. (2010). Stationary phase in gram-negative bacteria. *FEMS Microbiology Reviews*, *34*(4), 476–495. https://doi.org/10.1111/J.1574-6976.2010.00213.X

Nitzan, Y., Dror, R., Ladan, H., Malik, Z., Kimel, S., & Gottfried, V. (1995). Structure-activity relationship of porphines for photoinactivation of bacteria. *Photochemistry and Photobiology*, *62*(2), 342–347. https://doi.org/10.1111/J.1751-1097.1995.TB05279.X

Obata, M., Hirohara, S., Tanaka, R., Kinoshita, I., Ohkubo, K., Fukuzumi, S., Tanihara, M., & Yano, S. (2009). In vitro heavy-atom effect of palladium(II) and platinum(II) complexes of pyrrolidine-fused chlorin in photodynamic therapy. *Journal of Medicinal Chemistry*, *52*(9), 2747–2753. https://doi.org/10.1021/JM8015427

Oliveira, A., Almeida, A., Carvalho, C. M. B., Tomé, J. P. C., Faustino, M. A. F., Neves, M. G. P. M. S., Tomé, A. C., Cavaleiro, J. A. S., & Cunha, A. (2009). Porphyrin derivatives as photosensitizers for the inactivation of Bacillus cereus endospores. *Journal of Applied Microbiology*, *106*(6), 1986–1995. https://doi.org/10.1111/J.1365-2672.2009.04168.X

Pandey, R., Mishra, S. K., & Shrestha, A. (2021). Characterisation of ESKAPE Pathogens with Special Reference to Multidrug Resistance and Biofilm Production in a Nepalese Hospital. *Infection and Drug Resistance*, *14*, 2201–2212. https://doi.org/10.2147/IDR.S306688

Paterson, D. L., & Bonomo, R. A. (2005). Extended-spectrum beta-lactamases: a clinical update. *Clinical Microbiology Reviews*, *18*(4), 657–686. https://doi.org/10.1128/CMR.18.4.657-686.2005

Prasad, A. S. B., Shruptha, P., Prabhu, V., Srujan, C., Nayak, U. Y., Anuradha, C. K. R., Ramachandra, L., Keerthana, P., Joshi, M. B., Murali, T. S., & Satyamoorthy, K. (2020). Pseudomonas aeruginosa virulence proteins pseudolysin and protease IV impede cutaneous wound healing. *Laboratory Investigation; a Journal of Technical Methods and Pathology*, *100*(12), 1532–1550. https://doi.org/10.1038/S41374-020-00478-1

Ragàs, X., Agut, M., & Nonell, S. (2010). Singlet oxygen in Escherichia coli: New insights for antimicrobial photodynamic therapy. *Free Radical Biology & Medicine*, *49*(5), 770–776. https://doi.org/10.1016/J.FREERADBIOMED.2010.05.027

Ragàs, X., He, X., Agut, M., Roxo-Rosa, M., Gonsalves, A. R., Serra, A. C., & Nonell, S. (2013). Singlet oxygen in antimicrobial photodynamic therapy: photosensitizer-dependent production and decay in E. coli. *Molecules (Basel, Switzerland)*, *18*(3), 2712–2725. https://doi.org/10.3390/MOLECULES18032712

Rapozzi, V., Zorzet, S., Zacchigna, M., Della Pietra, E., Cogoi, S., & Xodo, L. E. (2014). Anticancer activity of cationic porphyrins in melanoma tumour-bearing mice and mechanistic in vitro studies. *Molecular Cancer*, *13*(1). https://doi.org/10.1186/1476-4598-13-75

Reddi, E., Ceccon, M., Valduga, G., Jori, G., Bommer, J. C., Elisei, F., Latterini, L., & Mazzucato, U. (2002). Photophysical Properties and Antibacterial Activity of Meso-substituted Cationic Porphyrins¶. *Photochemistry and Photobiology*, *75*(5), 462–470. https://doi.org/10.1562/0031-8655(2002)0750462PPAAAO2.0.CO2

Reynoso, E., Ferreyra, D. D., Durantini, E. N., & Spesia, M. B. (2019). Photodynamic inactivation to prevent and disrupt Staphylococcus aureus biofilm under different media conditions. *Photodermatology, Photoimmunology & Photomedicine*, *35*(5), 322–331. https://doi.org/10.1111/PHPP.12477

Rice, L. B. (2008). Federal Funding for the Study of Antimicrobial Resistance in Nosocomial Pathogens: No ESKAPE. *The Journal of Infectious Diseases*, *197*(8), 1079–1081. https://doi.org/10.1086/533452

Rodriguez-Mozaz, S., Chamorro, S., Marti, E., Huerta, B., Gros, M., Sànchez-Melsió, A., Borrego, C. M., Barceló, D., & Balcázar, J. L. (2015). Occurrence of antibiotics and antibiotic resistance genes in hospital and urban wastewaters and their impact on the receiving river. *Water Research*, *69*, 234–242. https://doi.org/10.1016/J.WATRES.2014.11.021

Rosenberg, A., Sinai, L., Smith, Y., & Ben-Yehuda, S. (2012). Dynamic expression of the translational machinery during Bacillus subtilis life cycle at a single cell level. *PloS One*, *7*(7). https://doi.org/10.1371/JOURNAL.PONE.0041921

Sabri, N. A., Schmitt, H., Van Der Zaan, B., Gerritsen, H. W., Zuidema, T., Rijnaarts, H. H. M., & Langenhoff, A. A. M. (2020). Prevalence of antibiotics and antibiotic resistance genes in a wastewater effluent-receiving river in the Netherlands. *Journal of Environmental Chemical Engineering*, *8*(1), 102245. https://doi.org/10.1016/J.JECE.2018.03.004

Sanchez, D. P., Tookes, H., Pastar, I., & Lev-Tov, H. (2021). Wounds and Skin and Soft Tissue Infections in People Who Inject Drugs and the Utility of Syringe Service Programs in Their Management. *Advances in Wound Care*, *10*(10), 571–582. https://doi.org/10.1089/WOUND.2020.1243

Schulz, S., Ziganshyna, S., Lippmann, N., Glass, S., Eulenburg, V., Habermann, N., Schwarz, U. T., Voigt, A., Heilmann, C., Rüffer, T., & Werdehausen, R. (2022). The Meta-Substituted Isomer of TMPyP Enables More Effective Photodynamic Bacterial Inactivation than Para-TMPyP In Vitro. *Microorganisms*, *10*(5). https://doi.org/10.3390/MICROORGANISMS10050858

Seier-Petersen, M. A., Jasni, A., Aarestrup, F. M., Vigre, H., Mullany, P., Roberts, A. P., & Agersø, Y. (2014). Effect of subinhibitory concentrations of four commonly used biocides on the conjugative transfer of Tn916 in Bacillus subtilis. *The Journal of Antimicrobial Chemotherapy*, *69*(2), 343–348. https://doi.org/10.1093/JAC/DKT370

Sezonov, G., Joseleau-Petit, D., & D'Ari, R. (2007). Escherichia coli physiology in Luria-Bertani broth. *Journal of Bacteriology*, *189*(23), 8746–8749. https://doi.org/10.1128/JB.01368-07

Sharma, B., Thakur, V., Kaur, G., & Chaudhary, G. R. (2020). Efficient Photodynamic Therapy against Gram-Positive and Gram-Negative Bacteria Using Rose Bengal Encapsulated in Metallocatanionic Vesicles in the Presence of Visible Light. *ACS Applied Bio Materials*, *3*(12), 8515–8524. https://doi.org/10.1021/ACSABM.0C00901

Skwor, T. A., Klemm, S., Zhang, H., Schardt, B., Blaszczyk, S., & Bork, M. A. (2016). Photodynamic inactivation of methicillin-resistant Staphylococcus aureus and Escherichia coli: A metalloporphyrin comparison. *Journal of Photochemistry and Photobiology. B, Biology*, *165*, 51–57. https://doi.org/10.1016/J.JPHOTOBIOL.2016.10.016

Steven, B., Briggs, G., McKay, C. P., Pollard, W. H., Greer, C. W., & Whyte, L. G. (2007). Characterization of the microbial diversity in a permafrost sample from the Canadian high Arctic using culture-dependent and culture-independent methods. *FEMS Microbiology Ecology*, *59*(2), 513–523. https://doi.org/10.1111/J.1574-6941.2006.00247.X

Sułek, A., Pucelik, B., Kobielusz, M., Barzowska, A., & Dąbrowski, J. M. (2020). Photodynamic Inactivation of Bacteria with Porphyrin Derivatives: Effect of Charge, Lipophilicity, ROS Generation, and Cellular Uptake on Their Biological Activity In Vitro. *International Journal of Molecular Sciences*, *21*(22), 1–34. https://doi.org/10.3390/IJMS21228716

Surur, A. K., Momesso, V. M., Lopes, P. M., Ferrisse, T. M., & Fontana, C. R. (2022). Assessment of synergism between enzyme inhibition of Cu/Zn-SOD and antimicrobial photodynamic therapy in suspension and E. coli biofilm. *Photodiagnosis and Photodynamic Therapy*, *41*. https://doi.org/10.1016/J.PDPDT.2022.103185

Tacconelli, E., Carrara, E., Savoldi, A., Harbarth, S., Mendelson, M., Monnet, D. L., Pulcini, C., Kahlmeter, G., Kluytmans, J., Carmeli, Y., Ouellette, M., Outterson, K., Patel, J., Cavaleri, M., Cox, E. M., Houchens, C. R., Grayson, M. L., Hansen, P., Singh, N., … Zorzet, A. (2018). Discovery, research, and development of new antibiotics: the WHO priority list of antibiotic-resistant bacteria and tuberculosis. *The Lancet. Infectious Diseases*, *18*(3), 318–327. https://doi.org/10.1016/S1473-3099(17)30753-3

Tan, Z., Qi, X., Gu, L., Bao, C., Tang, F., & Zhu, Y. (2014). Molecular characterization of Bacillus anthracis directly from patients' eschar and beef in an anthrax outbreak in Jiangsu Province, China, 2012. *The American Journal of Tropical Medicine and Hygiene*, *91*(3), 574–576. https://doi.org/10.4269/AJTMH.13-0633

Thorpe, K. E., Joski, P., & Johnston, K. J. (2018). Antibiotic-Resistant Infection Treatment Costs Have Doubled Since 2002, Now Exceeding $2 Billion Annually. *Health Affairs (Project Hope)*, *37*(4), 662–669. https://doi.org/10.1377/HLTHAFF.2017.1153

Van Boeckel, T. P., Gandra, S., Ashok, A., Caudron, Q., Grenfell, B. T., Levin, S. A., & Laxminarayan, R. (2014). Global antibiotic consumption 2000 to 2010: An analysis of national pharmaceutical sales data. *The Lancet Infectious Diseases*, *14*(8), 742–750. https://doi.org/10.1016/S1473-3099(14)70780-7

V.T, A., Paramanantham, P., Sruthil, S. L., Sharan, A., Syed, A., Bahkali, N. A., Alsaedi, M. H., K., K., & Busi, S. (2019). Antimicrobial photodynamic activity of toluidine blue-carbon nanotube conjugate against Pseudomonas aeruginosa and Staphylococcus aureus - Understanding the mechanism of action. *Photodiagnosis and Photodynamic Therapy*, *27*, 305–316. https://doi.org/10.1016/J.PDPDT.2019.06.014

Wasson, C. J., Zourelias, J. L., Aardsma, N. A., Eells, J. T., Ganger, M. T., Schober, J. M., & Skwor, T. A. (2012). Inhibitory effects of 405 nm irradiation on Chlamydia trachomatis growth and characterization of the ensuing inflammatory response in HeLa cells. *BMC Microbiology*, *12*. https://doi.org/10.1186/1471-2180-12-176

World Health Organization. (2017, February 17). *WHO publishes list of bacteria for which new antibiotics are urgently needed*. https://www.who.int/news/item/27-02-2017-who-publishes-list-of-bacteria-for-which-new-antibiotics-are-urgently-needed

World Health Organization (WHO). (2021, November 17). *Antimicrobial resistance*. https://www.who.int/news-room/fact-sheets/detail/antimicrobial-resistance

Xiao, Q., Mai, B., Nie, Y., Yuan, C., Xiang, M., Shi, Z., Wu, J., Leung, W., Xu, C., Yao, S. Q., Wang, P., & Gao, L. (2021). In Vitro and In Vivo Demonstration of Ultraefficient and

Broad-Spectrum Antibacterial Agents for Photodynamic Antibacterial Chemotherapy. *ACS Applied Materials & Interfaces*, *13*(10), 11588–11596. https://doi.org/10.1021/ACSAMI.0C20837

Xu, Z., Gao, Y., Meng, S., Yang, B., Pang, L., Wang, C., & Liu, T. (2016). Mechanism and In Vivo Evaluation: Photodynamic Antibacterial Chemotherapy of Lysine-Porphyrin Conjugate. *Frontiers in Microbiology*, *7*(MAR). https://doi.org/10.3389/FMICB.2016.00242

Xuan, W., Huang, L., Wang, Y., Hu, X., Szewczyk, G., Huang, Y. Y., El-Hussein, A., Bommer, J. C., Nelson, M. L., Sarna, T., & Hamblin, M. R. (2019). Amphiphilic tetracationic porphyrins are exceptionally active antimicrobial photosensitizers: in vitro and in vivo studies with the free-base and Pd-chelate. *Journal of Biophotonics*, *12*(8), e201800318. https://doi.org/10.1002/JBIO.201800318

Zhang, Y., Gu, A. Z., He, M., Li, D., & Chen, J. (2017). Subinhibitory Concentrations of Disinfectants Promote the Horizontal Transfer of Multidrug Resistance Genes within and across Genera. *Environmental Science & Technology*, *51*(1), 570–580. https://doi.org/10.1021/ACS.EST.6B03132

Zulk, J. J., Clark, J. R., Ottinger, S., Ballard, M. B., Mejia, M. E., Mercado-Evans, V., Heckmann, E. R., Sanchez, B. C., Trautner, B. W., Maresso, A. W., & Patras, K. A. (2022). Phage Resistance Accompanies Reduced Fitness of Uropathogenic Escherichia coli in the Urinary Environment. *MSphere*, *7*(4). https://doi.org/10.1128/MSPHERE.00345-22